PALACKÝ UNIVERSITY OLOMOUC

Faculty of Science

Department of Physical Chemistry

Bachelor thesis

Graphene-based materials for electrochemical applications

Anna Krestová

Supervisor:	Kumara Ramanatha Datta Kasibhatta, Ph.D.
Consultant:	Ing. Veronika Urbanová, Ph.D.
Study program:	B1407 Chemistry
Study course:	Applied Chemistry
Form of study:	Daily attendance

Olomouc 2016

Declaration of the author

I declare that I have worked out this thesis by myself under supervision of K. K. R. Datta, Ph.D. All references and information sources used in this thesis are properly cited.

I agree with the accessibility of my thesis in the library of Physical Chemistry Department, Faculty of Science, Palacký University in Olomouc.

Olomouc, April 2016 ……

Anna Krestová

Acknowledgement

There are a number of people who have contributed to make this thesis done and to whom I would like to greatly thank. At first I thank my supervisor K. K. R Datta for his professional advice, patience and devoted time through whole area of working and learning the chemistry of graphene related materials.

I am also thankful to Veronika Urbanová as she introduced me the nature and exploitation of electrochemistry techniques and from whom I got lots of valuable advice and dedicated help during the measurements.

My thanks belong to Michal Otyepka, who enabled and helped in arrangement of my thesis background in both Regional Center of Advanced Technologies and Materials and Department of Physical Chemistry, which gave me great profit.

Sincerely, I would like to thank to Regional Center of Advanced Technologies and Materials and Department of Physical Chemistry for facilitating of my work and to all its employees who helped me with measuring and understanding various analyses, individually Claudia O. Aparicio for measuring the XRD patterns of all my samples, Ariana Fargašová for providing me an excursion to Raman spectroscopy during the measurements, also Petra Bazgerová for providing me SEM and TEM spectroscopy analyses and EDS evaluations in my presence. Many thanks belong to Martin Petr for providing me XPS analysis and appropriate data and Juri Ugolotti for CHNS analysis. Finally, I would like to thank Eva Otyepková for her willingness and help with lyophilization procedure and Bohuslav Drahoš from Department of Analytical Chemistry who provided me liquid nitrogen for lyophilization.

My great thanks belong to my family for the support in the study.

Bibliographical identification

Author´s first name and surname:	Anna Krestová
Title:	Graphene-based materials for electrochemical applications
Department:	Department of Physical Chemistry
Type of thesis:	Bachelor
Supervisor:	Kumara Ramanatha Datta Kasibhatta, Ph.D.
Consultant:	Ing. Veronika Urbanová, Ph.D.
The year of presentation:	2016

Abstract:

The functionalization of graphene has received special interest among diverse research groups due to its implications in optics, electronics and energy. For example, doping of nitrogen in graphene creates binding sites, tunable electrical properties and improved catalytic activity as compared to pristine graphene. In this work, the aim was to synthesize hybrid nanostructures based on the reduction of graphene oxide (GO) with nitrogen precursor resulting in nitrogen doped reduced graphene oxide (rGO-N). Also rGO/MoS_2 hybrid by solvothermal reduction of GO with ammonium molybdate and sulfur powder was prepared. The obtained materials were characterized using various spectroscopic and microscopic techniques to understand the chemistry and subsequently testing them for electrochemical and sensing properties when used for modification of electrode´s surface. The results have proven enhanced electrochemical responses for both hybrids and modification with rGO-N performed catalytic activities for ascorbic acid and dopamine detection and separated detection in their mixture.

Key words:	Graphene, graphene oxide, nitrogen doping, MoS_2, aerogels, electro-sensing
Number of pages:	53
Number of appendix:	0
Language:	English

List of Abbreviations

GO – Graphene oxide

rGO – Reduced graphene oxide

rGO-N – Nitrogen doped reduced graphene oxide

rGO/MoS_2 – Reduced graphene oxide/MoS_2 hybrid

CVD – Chemical vapor deposition technique

GH-N – Nitrogen doped reduced graphene oxide hydrogel

GA-N – Nitrogen doped reduced graphene oxide aerogel

ORR – Oxygen reduction reaction

HER – Hydrogen evolution reaction

XRD – X-ray diffraction

SEM – Scanning electron microscopy

TEM – Transmission electron microscopy

EDS – Energy dispersive X-ray spectroscopy

FTIR – Fourier transform infra-red spectroscopy

XPS – X-ray photoelectron spectroscopy

CV – Cyclic voltammetry

EIS – Electrochemical impedance spectroscopy

EDA – Ethylenediamine

CHNS – Analyzer for elemental content of carbon, nitrogen, hydrogen and sulfur

GCE – Glassy carbon electrode

AA – Ascorbic acid

DA – Dopamine

PBS – Phosphate buffer solution

CNTs – Carbon nanotubes

Contents

1. Introduction

Recently discovered two-dimensional graphene material, has been attracting huge interest among scientists all over the world due to its exceptional properties. The reason is hidden in its unique structure of honeycomb lattice composed of carbon atoms. Graphene is one atom thick planar carbon sheet, flexible, and is a basic building block for graphitic materials of other dimensionalities (*e.g.* fullerene and CNTs). The electrons in graphene move along the lattice with almost the speed of light. The electrical conductance of graphene is comparable to that of copper and thermal conductivity is better than that of silver[1]. Due to all these properties observed in unimaginable nanoscale dimensions, first suggestions of its applicability led to the nano-opto-electronics research of transparent conductors, transistors, batteries, sensors and liquid crystal displays[2]. Currently various research groups are involved in the chemical functionalization of graphene to create novel graphene derivatives and composites depending on the type of application.

There are several fascinating derivatives of graphene materials such as graphene oxide, fluorographene, graphane which show remarkable properties and applications. Graphene can be covalently modified by oxygen functionalities to form hydrophilic graphene oxide (GO). The attachment of fluorine atoms covalently bonded to graphene creates fluorographene and it can be isolated by liquid–phase exfoliation of graphite fluoride[3]. Reaction of hydrogen with graphene *via* hydrogen plasma treatment gives rise to graphane[4]. These derivatives of graphene show interesting magnetic, optical and electrical properties as compared to pristine graphene. The crucial change for such functionalized graphenes is the band gap modification depending on the heteroatom content. Among the mentioned graphene derivatives, GO due to easy synthetic approach and handling is extensively used in fields like biology, catalysis and packaging.

GO is promising graphene derivative due to its oxygen functionalities providing water dispersibility[5,6,7]. GO has aromatic regions very similar to that of graphene, however sp^2 hybridization of carbon is significantly less as compared to graphene. Most importantly, GO has oxygen containing functionalities which help in binding other molecules for the preparation of composites. The oxygen functionalities are also responsible for suppressed electrical conductivity. The electrical conductivity can be improved by chemical or thermal treatment of GO to obtain reduced graphene oxide (rGO).

The current research in rGO is focused on tuning the processing methods for obtaining rGO in multi-dimensional architectures, such as hydrogels and aerogels due to the fact that pure GO solution suffers from fast and significant sheet stacking and low surface area[7]. The properties of such composites are found to be significantly multiplied due to higher and moldable volume, larger surface area and improved ultrafast charge mobility, which is promising for enhanced ion adsorption capacity of batteries and storage devices[8,9,10]. Despite graphene has electrically neutral character and GO is considered as insulator, their energy band gap may be adjusted by doping with heteroatoms[11] and other 2D material[12]. Such combination offers synergetic effect in electrical performance.

This work was focused on synthesis, characterization and testing two specific rGO systems that are capable of showing remarkable electrochemical applicability. First system was nitrogen doped reduced graphene oxide aerogel (rGO-N) with porous structure with nitrogen containing functional groups contributing to electrical conductivity[13]. The second was three-dimensional hybrid of MoS_2 nanostructures attached on reduced graphene oxide sheets (rGO/MoS_2) capable of outstanding enhancement in electrochemical activities as well owing to the facilitated access to MoS_2 active sites[14].

2. Graphene: Two-dimensional crystal of carbon

Graphene is a 2D crystalline form of carbon that was not observed in the carbon family for decades. It is represented by a sheet that consists of the repetition of basic units which are formed of six carbon atoms. These are shaped to form a hexagon, which extend in plane forming honeycomb-like carbon lattice. The formation corresponds to sp^2 hybridization of carbon atoms and the height of such lattice corresponds to height of carbon atom which is only 0.34 nm[15]. The atoms of two neighbouring layers are situated directly above each other as in graphite[16].

For material having only two dimensions, its nature and behaviour is completely different from its three-dimensional (3D) counterparts. Thermal vibrations with such thickness may cause great dislocation of the atoms in the network. Additionally, the lower thickness causes decrease in the melting point and therefore decline of stability which naturally results in forming 3D crystallite. That's why scientists believed for long history, that such materials are thermodynamically unstable and nobody could synthetize them[2,15,17]. Brilliant idea of isolating existing 2D material from bulk, instead of forming 2D material from

the bottom-up approach which needs crystallite substrate to form that, led to the destruction of the weak van der Waals forces between each integral 2D layer and the first isolation of particular single layer of graphene. The idea occurred to Andre Geim and Konstantin Novoselov at the University of Manchester in October 2004. Today commonly known mechanical exfoliation performed by multiple tape-tricking of graphite flakes resulted in Nobel Prize in Physics "for ground-breaking experiments regarding the two-dimensional material graphene" for which the developers were awarded[18]. Thanks to this foundation, nowadays we know many other ways of preparation and/or isolation of 2D materials and their nature and potential which culminate their use for modern future devices and applications.

Theoretical presumptions of instability of 2D planar sheets are justified and remain valid. Nonetheless, graphene was proved to be stable because it is capable to hinder the thermal fluctuations and minimize the free energy[2]. Despite it is seemingly planar; in fact, it is crumpled or wrinkled throughout. This is the key factor which facilitates it to resist even the room temperature conditions[2, 19]. The structural model of graphene monolayer is shown in Figure 1. Nevertheless, to the stability of all 2D crystals contributes, also the minimal height and strong bonding between the in-plane atoms. These all factors help to supress the total free energy[2].

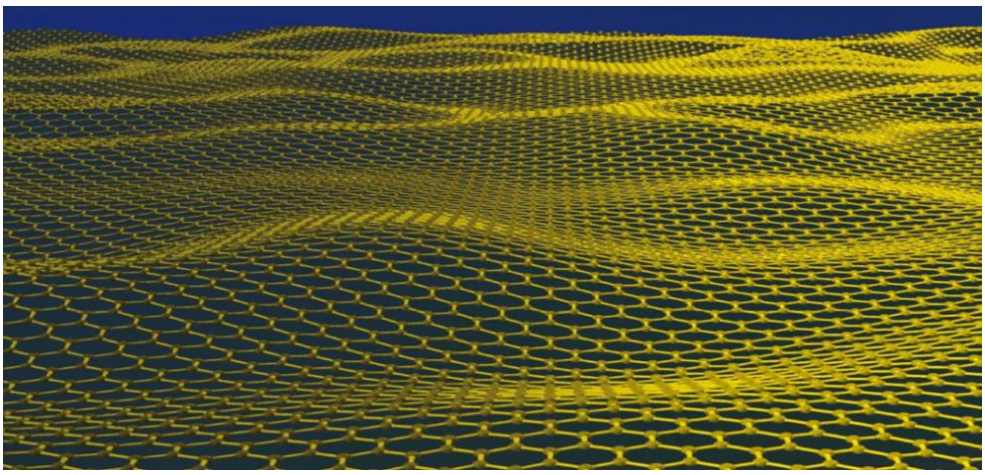

Figure 1. Structural model of graphene monolayer with slightly wrinkled character. [Adapted from ref. 20, author: J. Meyer]

2.1.Graphene´s merits

For further classification of graphene, let's focus deeply on the structural features. Carbon has 4 valence electrons and 3 of them are covalently connected *via* σ-bonds to 3 other neighbouring carbon atoms, which lie in the graphene plane. While the 4th electron, occupying the $2p_z$ σ-orbital is situated perpendicularly to the plane. These out-of-plane electrons are responsible for formation of valence and conductive band, above and below the lattice and these are the most important for understanding the electronic properties of graphene. As shown in Figure 2, Fermi level lies between valence electrons and conductive holes. The meeting points of electrons and holes results in zero bandgap semiconducting behaviour in graphene monolayer. It also clearly shows that electrons and holes form linear dispersion in the area of Fermi level. Hence, the electron energy goes linearly along the wave vector as well, giving them no effective mass[2,17]. Regular and perfect crystal lattice enables electrons to move through it extremely easily and fast. This culminates in the electron propagation through the network with the speed almost reaching the speed of light [20]. With this fact it should be also pointed that graphene may be considered as one single, two or multi-layered. In such tiny dimensions, with every seemingly insignificant change, each property differs extensively. Especially electronic properties of graphene are strictly dependent on the number of layers. Lots of graphene layers structured into bulk graphite act like a semi-metal whereas monolayer is semiconductor. Hence, controlling the number of layers may be used to adjusting the electrical behavior[21]

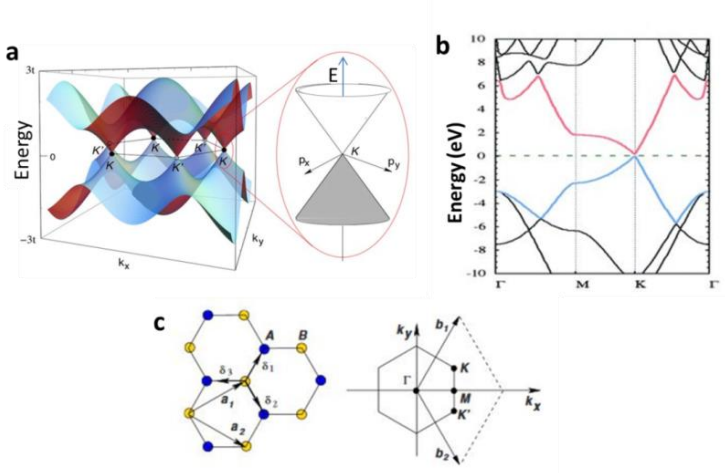

Figure 2. a) Fermi level is formed by connection of K and K´ points of the first Brillouin zone, which can be seen in K and K´ points divide valence and conductive energy bands by direct transport which leads to zero band gap in energy spectrum illustrated in b), c) The first Brillouin zone of graphene. [Adapted from refs a) 23; b) 24; c) 21]

Yet another graphene exceptional merit is the nature of its charge carriers with the mobility as high as 15 000 $cm^2 \cdot V^{-1} \cdot s^{-1}$ at room temperature[2], leaving the best conductivity of copper far behind. Quantum Hall effect in graphene may be, therefore, seen unusually even at room temperature, which was inconsiderable before[17,21]. Apart from the electronic, thermal and mechanical properties have their origins also in wide π-conjugation plane, they are affected by anisotropy. Significantly easier propagation of conductivity is facilitated through in-plane direction due to strong π interactions of π orbitals than perpendicular to the layers, where only weak van der Waals forces are present[15]. Theoretically, graphene possesses in-plane thermal conductivity[1] overcoming that of silver, copper and even carbon nanotubes, reaching to 5 000 $W \cdot m^{-1} \cdot K^{-1}$. Mechanical resistance is reflected in the breaking strength of 42 $N \cdot m^{-1}$, overcrossing the strength of the same thick sheet of steel by a factor of hundred[1]. Also, graphene absorbs only 2.3% of white light[1,19] that is induced by the aromatic character with the maximal absorption at 268 nm in visible region[1,19]. Theoretical surface area of pristine graphene[8] reaches to 2 630 $m^2 \cdot g^{-1}$. At the same time, its density prevents the transmittance for gases [20]. Interestingly, features such as stiffness and flexibility makes graphene unbeatable for various kinds of industrial exploitation.

2.2. Preparation of graphene

Various methods of graphene production were investigated since its discovery. Basically, there are two important ways to obtain graphene including physical and chemical approaches.

Physical ways of graphene isolation include historical method for production of graphene by mechanical cleavage of graphite[1,15,17], burning off the silicon carbide surface used by De Heer´s group, isolation of thin graphene sheets from graphite using atomic force microscope tip applied on its surface proposed by Kim *et al.* or synthesis from nanodiamonds according to Affoune *et al.*[1,21]. In solid state, graphene monolayer can be grown on the crystal substrate. Similarly to this approach chemical vapor deposition technique (CVD) is also implemented[2]. Metallic organic materials are very favorable substrates due to their easy isolation from graphene layers that have grown on them[22]. Alternatively, thermal decomposition of silicon carbide crystals yields graphene films[2,20]. Schematic illustration of mechanical exfoliation of graphite is shown in Figure 3.

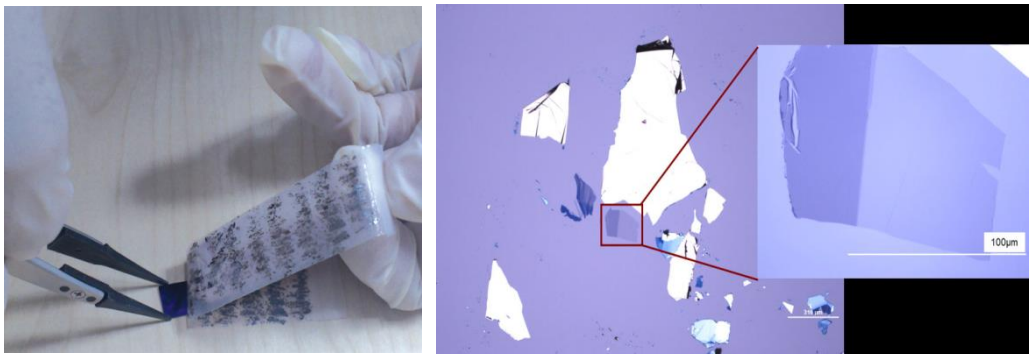

Figure 3. Mechanical cleavage of highly ordered pyrolytic graphite (HOPG) by scotch-tape technique. This method was used during the first isolation of single graphene sheet in 2004 (left). The picture from optical microscope. graphene is deposited on the oxidized silicon wafer (right). [Adapted from ref. 25 and 26)]

Chemical routes to obtain graphene include application of ultrasound to graphite powder in organic solvents[19,27] resulting in the exfoliation of graphite, such solution consists of very less single and majority of few-layered graphene sheets[17,19]. Another approach of preparing graphene starts from graphene oxide (GO). Reduction of oxygen groups can be induced by many ways, typically thermally, at reduction temperatures about 2000 °C[28], chemically with hydrazine hydrate[29] and sodium borohydride[30], or electrochemically[8]. Similarly as in the case of ultrasonic cleavage, these methods lead to reduced GO (rGO) suitable for further functionalization, owing to the residual oxygen groups, which are never completely destroyed from the graphene plane. Figure 4 illustrates the process of chemical exfoliation and the corresponding graphene sheets obtained and characterized by microscopic techniques.

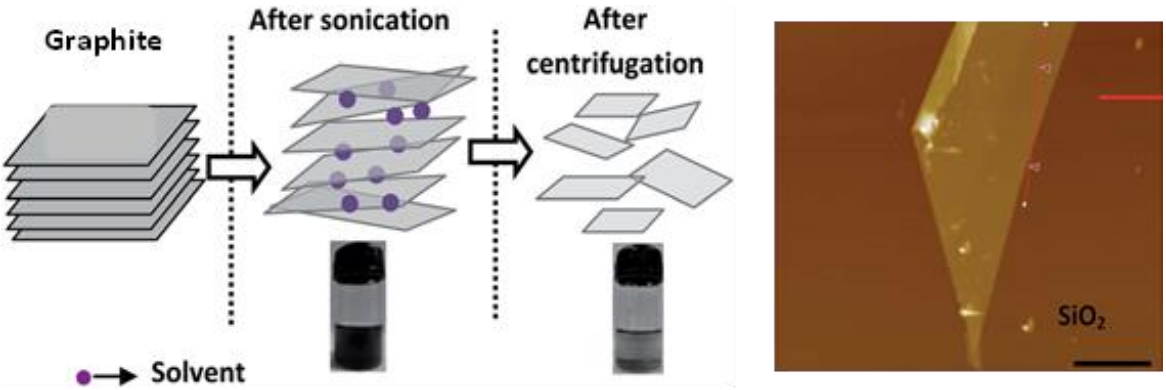

Figure 4. Scheme of chemical exfoliation of graphite with solvents. Solvents may be toluene, chlorobenzene, acetone, DMF, N,N-dimethylformamaide *etc*. (left). Atomic force microscopic image of graphene exfoliated in toluene (right). [Adapted from ref.27]

3. The chemistry of graphene oxide

Comprehensive investigations of graphene monolayer have proposed promising theoretical properties for advanced supercapacitors, batteries and electrochemical sensing applications according to aforementioned properties. However, in reality, single graphene layers naturally tend to stack back to graphite form and properties of condensed layered betray graphene direct usage[7]. Nowadays, functionalization of graphene network with such additives that compensate the deficiency is of great interest. In all cases, foremost is to prepare graphene intermediates which are dispersible and stable in the most possible kinds of solvents, which both keeps the graphene sheets loose rather than stacked and facilitates following functionalization[31]. GO used as graphene intermediate for modification was established as the most ideal, which was already confirmed by the highest percentages of its usage. GO solution serves as anti-stacking agent as a consequence of repulsive forces between ionized oxygen rich functionalities[7]. Negative charged surface also protects the stability of the solution, which was confirmed by highly negative values of zeta potential measured in GO water solution by Wallace *et al.*[7] and the results are shown in Figure 5.

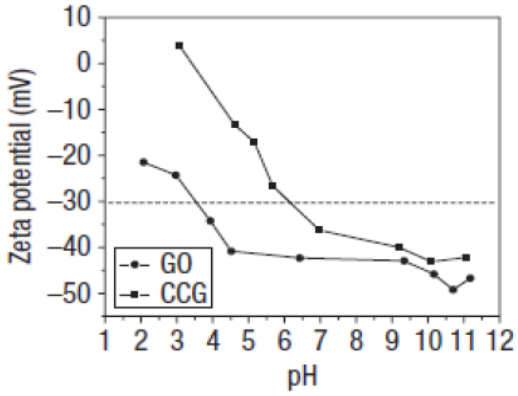

Figure 5. Study of the zeta potential of GO water solution and its dependence on pH values. Highly negative values under -30 mV in majority of pH range indicates stable solution. [Adapted from ref.7]

Graphene plane in this model contains multiple oxygen containing functional groups (such as epoxy-, hydroxyl-, carbonyl- or carboxyl- groups) bonded covalently to its surface[32]. These reactive sites are distributed along the plane, presumably with the highest concentration along the edges[32,33]. Oxygen functional groups significantly improve graphene's reactivity. They are essential for exposing graphene sheets, for participating in chemical reactions as well as enabling facile water-dispersibility[6]. Therefore, GO received a key role of ideal initial material for various functionalization methods, particularly in its dispersion phase. Synthetic

methods employed for the preparation of GO from graphite precursor are summarized in Table 1, and Figure 6 illustrates mechanism of GO formation during the most common Hummer´s method of synthesis[34,35].

Table 1. Summary of the development of GO synthesis

Year	Author	Reagents	
1859	Brodie	Graphite flakes	fuming HNO_3 + $KClO_3$
1898	Staudenmaier		fuming HNO_3 + conc.H_2SO_4 + $KClO_3$
1937	Hofmann		conc. HNO_3 + conc.H_2SO_4 + $KClO_3$
1958	Hummers		conc.H_2SO_4 + $NaNO_3$ + $KMnO_4$

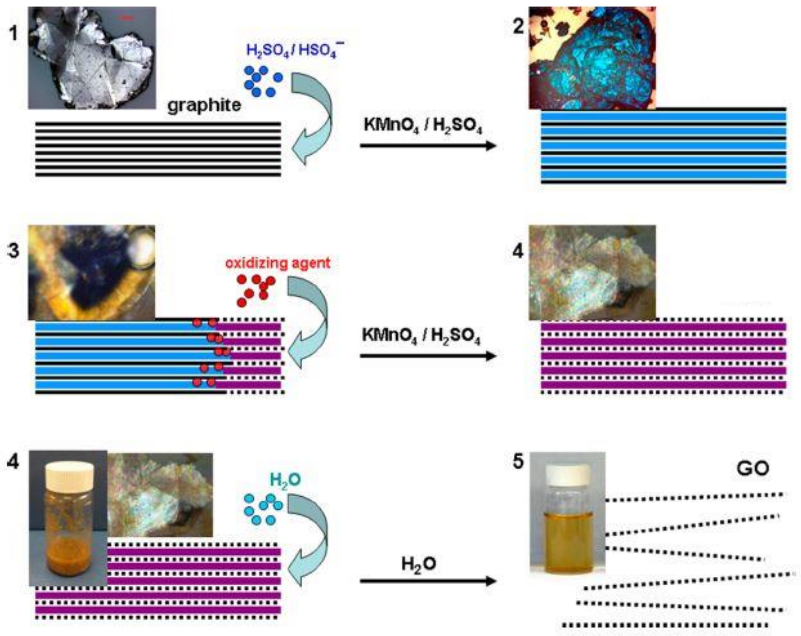

Figure 6. Schematic mechanism showing GO formation. The process consists of three steps: acidic intercalation of sulfuric acid into graphite flakes in step 1 extends interlayer distance; potassium permanganate with sodium nitrate penetrates between the layers leading to the oxidation in step 2; in the step 3, water treatment hydrolyses the sulfate linking. [Adapted from ref. 6]

Nevertheless, even if graphene sheets are exposed and stable in GO water dispersion, low electrical conductivity caused by oxygen functionalities keeps the less exploitation[7,8]. It is known, that reduction of the oxygen groups can at least partially recover electrical conductivity[5,7,32]. This viewpoint resulted in many methods developed for reduction of GO,

which was mentioned before as one of the ways to prepare graphene. Predictably, all these reduction reactions somehow affect the quality of products by *e.g.* induced heteroatomic impurities[36] as well as damaged sp^2 network or ineffective large scale production, respectively[5]. Since hydrophilic restacking occurs after removal of oxygen groups there has to be optimal additional conditions to avoid the stacking and to facilitate higher order structures. Regarding electrochemical application, the probable tuning should result in great absorption and charge transfer of the final structure[8].

3.1. Reduced graphene oxide frameworks

GO based frameworks like foams, aerogels and spongy 3D composites have attracted recent scientific interest because they possess much lower density and weight than hydrogels, they show moldable volume morphology and facilitate enhanced multidimensional electron transport pathways[13,37,38,39]. Therefore, freeze drying of hydrogel is induced to obtain aerogels with high surface area to volume ratio and ultra-light compressible structure[37,38,10,40,41]. Freeze-casting creates water ice crystals from the water molecules in the intrinsic pores. During subsequent vacuum drying these crystals are vaporized leaving air pores instead of them so the porous density is increased[41]. It is known that micro- and macro-porosity could be controlled by directing the temperature of (freeze) drying[42]. Graphene-based macroporous materials with low densities can be used as attractive substrates for electrodes[8,10,43], sorbent materials with remarkable absorption capacity and recyclability towards organic dyes and solvents[40], oils, heavy metals and also showing catalytic activities towards sorption of pollutants or low detection limits and advanced sensitivity of graphene sensors[39].

Hydrothermal reduction treatment takes advantage of un-balanced distribution of functionalities in GO surface and therefore is able to feasibly and in large scale adjust the GO structure into 3D hydrogel morphology[13,43], and thus hinder the GO stacking. GO structure decomposes (at temperatures of 60 – 80 °C)[44] forming thermally reduced GO. Such rGO is more conductive and at the same time, remained oxygen species are ready to participate in desire subsequent reactions[19,31]. In this light, hydrothermal synthesis method provides all the required conditions and can be easily freeze-dried into aerogel.

Aerogels, as well as hydrogels, are mechanically unstable and need reinforcement support[40,41,45]. Therefore, even before lyophilization, gel-like rGO is usually strengthened

non-covalently in polymer mixture (ethylenediamine), with multivalent metal ions (Li^+, Mg^{2+}) or biomolecules (DNA)[43], or polymerized covalently, *e.g.* by dopamine[46]. Simple immersion into ammonia solution before freeze-drying supports the mechanical toughness of final product[40]. The key aspect of the reactions is that sp^2 graphene lattice of the composite will not be further damaged[41].

Further tuning of aerogels, especially in adjusting electrical performance is feasible by heteroatoms doping[47], which was proved as one of the effects helping in GO reduction methods[36]. Though semiconducting graphene materials are obtained by fluorine doping[3], nitrogen or boron heteroatoms improve electrical conductivity[11]. Moreover, heterostructures may be constructed by combination of graphene layers with another 2D layered material[48]. Advantageous tuning leads to remarkable electrochemical behavior of final products. Specifically, electronegative nitrogen in N-doped rGO aerogels allows modulation of band gap[11] and MoS_2 provides more active sites exposed for enhanced kinetics of electron mobility[14,49]. This is why they show potential as modification materials for electrochemical sensing or catalytic systems[12,49,50].

4. Nitrogen-doped reduced graphene oxide

Nitrogen atom has five valence electrons and usually is trivalent; therefore a free electron pair makes it more electronegative. When N is incorporated to GO structure, the electrical conductivity and overall electrical properties are improved as a consequence of the free electron pair which contributes to more efficient electron transport along aromatic network.

Nitrogen doped graphene based materials were found to be promising for modification of electrodes, especially in the case of supercapacitors and electrochemical sensors, due to the possibility to tune the inner microporous structure by adjusting the amount of N source[13,37,55]. Unlike strong reductants, mild doping process facilitates partial reduction of GO and thus hinder the agglomeration and the final composite possesses with high specific area, allowing applicability in energy absorption or shock damping[37]. Demand on electrical applications, especially on batteries and transistors, are very dependent on enhanced properties achieved *via* N-doping, such as moldable band gap allowing moldable conductivity in addition to higher power capability, perfect cycle life and altered power density[13]. Nitrogen induces their faster charge/discharge rate and higher specific capacitance. Intercalated nitrogen atoms

support the charge storage and stability of the structure[55]. Electrochemical detection performance of currently used electrodes do not fulfill requirements for selectivity to detect desire analyte in mixture of interfering metabolites. Although common human liquids (blood serum, plasma, urine *etc*.) containing many components are daily evaluated and the need of stable and facilitated simultaneous separation of each component is very desirable. N-doped graphene based materials have potential to detect organic molecules and several biological objects abundant in human body[54,56]. Furthermore, there is a lot of research progress towards oxygen reduction reaction (ORR) using N-doped graphenes[38,53].

There are several methods used for N-doping with several nitrogen precursors. In general nitrogen is incorporated in graphene as graphitic, pyrrolic or pyridinic bond configurations[43]. For illustration, nitrogen sources like urea, melamine, pyrrole or ammonia was used to obtain composites employed with enhanced stability, electron mobility or electrochemical sensing activity[45,49].

N-doping of graphene involves diverse methodic ways of preparation and they are subsequently reflected in properties of final product. Amines are suitable sources for graphene functionalization, because they show reactivity with wide range of chemicals resulting in easy solubility in wide range of solvents[51]. Unconventional synthesis can be presented by arc discharge of graphite electrodes under the hydrogen, helium and pyridine or ammonia vapors as possible option according to Panchakarla *et al.*[52]. This method is based on molecular charge transfer and such functionalization highly affects and facilitates the band gap adjustment. Typically, pyridine or ammonia vapors are carried in H_2 and He gases to arc-chamber where two graphite electrodes (simple graphite cathode and graphite anode modified with additional metal oxides) are placed and where, after voltage and current incident (approximately 30 V and 30 A), gas-mixture discharges[19]. Pyridine vapors with or even without He carrying gas are capable of transformation of nanodiamonds into N-doped graphene as well[52].

CVD is further possibility how to prepare doped graphene-based materials applying most frequently methane and ammonia eventually ethylene/hydrogen mixture with ammonia on copper or modified Ni-coated SiO_2/Si or Cu/Si substrates under highly elevated temperatures ranging commonly between 800 to 1000 °C[19]. Advantageous is the possibility to

control the N:C content ratio *via* the N-gas flow rate modulation. This method yields high quality crystallites and fine surface[53].

Worth mentioning is pyrolysis method, where the principal is thermal annealing of GO/N-source mixture[19]. Valuable N-source is cyanamide, melamine, carbon nitride or urea. Advantageous point of this method was found to be in controlling the type of N configuration presented in doped composites by adjusting the temperature from 300 °C to 900 °C[54]. There is majority of pyridinic type in all used temperatures, whereas the pyrrolic and graphitic types exchange their representations. Temperatures about 300 °C induce majority of pyrrolic type and minority of graphitic type and in elevated temperature about 600 °C it is vice versa. At even higher 900 °C, the majority of observed types belong to pyridinic and graphitic type of N[54]. Moreover, with increasing temperature, increasing pressure is inducted and the greater expansion occurs. Subsequently, the specific surface area is increased as well[54]. This is valuable information from the electrochemical point of view, since N configurations show selectivity for redox reactions[19,53].

Hydrothermal treatment is one of the most promising approaches due to its mild, facile, low-cost and effective nature[40]. Hydrothermal treatment enables the incorporation of N-source during the reduction of GO[49]. As aforementioned, amines or any other N-containing molecule could serve as N-source and as the mechanical reinforcement[40]. Generally, simple mixing of nitrogen precursors with GO solution to assemble together hydrogel-like material is facilitated at temperatures about 180 °C[13,37,38]. Figure 7a illustrates the whole reaction process and Figure 7c shows how the amount of N-source affects the volume in N-doped graphene hydrogel (GH-N)[13]. This study also revealed the dependence of hydrogel volume on the type of N-source. Following freeze-drying converts hydrogel to aerogel. Apart from temperature based controlling over the pore size, Figure 7b demonstrates GH-N (N source is ammonia) freeze-dried into aerogel structure (GA-N) and interprets that lower volume and altered pore density of obtained GA-N is influenced by the concentration of applied N-source as well, as the concentration adjusts the ice point of water in GH-N in freeze-drying process, respectively[40]. Slightly different process introduces progressive chemical reduction of GO that is carried before thermal treatment with ammonia, which results in higher degree of substituted carbon atoms in plane network[19].

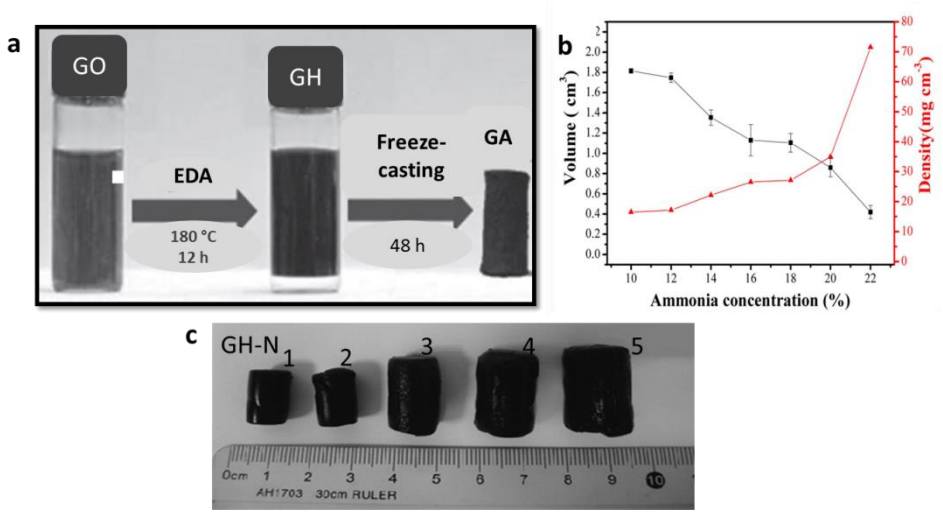

Figure 7. a) Illustration of synthesis steps leading from GO and ethylenediamine mixture through hydrothermal treatment to formation of graphene aerogel; b) Volumes and densities of GA-N samples with respect to N-source concentrations; c) Graphene hydrogel doped with ethylenediamine as nitrogen source (GH-N). Samples from 1 to 5 contain different amounts of ethylenediamine, rising from 2.5 to 20 µl. [Adapted from ref 13, 37and 40]

In this work, N-doped rGO aerogel was prepared by hydrothermal synthesis of ethyelenediamine (EDA) and GO followed by freeze drying. The amount of N was found to be 11at%. This was consequently used for characterization, testing and understanding its structural, functional and electrochemical properties.

5. MoS_2/rGO hybrid

Recent investigations show that various combinations of MoS_2 with GO exhibit excellent energy conversion performances when used as electrode coatings[12], their moldable volume and high specific area enhances lithium storage abilities and charge/discharge cycling in lithium-ion batteries and specific capacities of supercapacitors[14]. Such composites were also found to promote great electrocatalytic activities[57] or enhance electrochemical and (bio)sensing performance[12,58]. More preciously, enhanced electron transfer is ascribed to the synergetic effect in binding energy between MoS_2 and graphene sheets[59]. Consequently, lower resistance, stable and reversible capacities are determined. Since they are keeping high surface area and 3D conductive network, they are very sensitive for physiological metabolites and their showing detection in lower overpotentials[12]. For this reason they are suitable for biosensor construction where transport of detected information is facilitated by MoS_2 active sites[50].

Outstanding electrochemical catalytic behavior was recently attributed to N-doped graphene/MoS_2 hybrid, in which N creates n-type semiconducting behavior and MoS_2 involves p-type semiconducting properties[59]. Charge/discharge capacity and cycling performances as well as stability and catalytic activity highly increased with respect to unmodified graphene/MoS_2, especially regarding HER catalytic activity due to the synergetic electrical properties of N and MoS_2 that are conductively bonded[49,66]. Nevertheless, when reducing or other supporting agent is hydrazine or any other N-containing molecule, it may count as N source as well.

Generally, rGO/MoS_2 hybrids are promising catalysts for hydrogen evolution reaction (HER)[14,49,57,60]. Interest in HER has its roots in attempts for targeted production of hydrogen for utility as alternative and environmentally friendly replacement of fossil fuels [49]. Conveniently, hydrogen is generated in electrolysis of water; however, it needs effective and inexpensive catalyst. Separated MoS_2 sheets aggregate and thus their support is highly desirable[49]. It was revealed that 3D macrostructures of MoS_2/GO hybrids exhibit even more enhanced activities in HER catalysis and subsequently in all other electrochemical properties. Here we first focus on the structure and properties of MoS_2 followed by the synthetic approaches for the preparation of rGO/MoS_2 hybrid.

MoS_2

Molybdenum disulphide (MoS_2) is one of the typical representatives of two-dimensional (2D) rising layered materials. It ranges among transition metal dichalcogenides, which received significant importance since the discovery of graphene. Similarly, they were found to be easily exfoliated into monolayers. Attractive properties are rising from d-electrons and their quantum behavior[61], related to their nanometer size which is smaller than their wavelength and therefore leading to discrete energy levels and increment of excitation and binding energies[62]. Among its characteristics belong semiconductivity [61], high quality valley selective circular dichroism[60,63], and photoluminescence up to 50%[63].

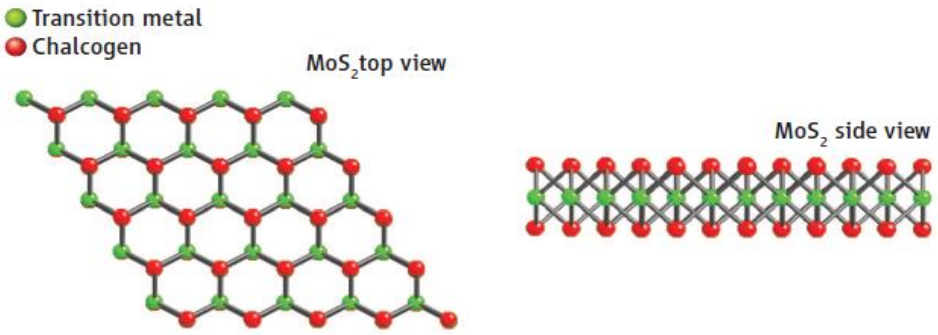

Figure 8. Structure of MoS_2 monolayer. [Adapted from ref. 104]

Monolayer MoS_2 has sandwich-like character. It is composed of two sheets of hexagonal sulphur (S) atoms while additional sheet of molybdenum (Mo) atoms is loaded between them. Top and side view of the atom formation is shown in Figure 8. In contrast to indirect band gap of bulk MoS_2, it changes into direct band gap in monolayer[61]. Likewise monolayer graphene, it exhibits similar structural periodicity and becomes flexible in 2D form[63]. The forces introduced throughout MoS_2 layers are of van der Waals character, thus weak, whereas the inner-layer bonds that connect S and Mo together are covalent[55] facilitating electron transfer. Despite of that, MoS_2 provides one electrical characteristic that is lacking in graphene. MoS_2 is semiconductor with band gap of 1.9 eV[60], thus it do not have to be further adjusted. Furthermore, MoS_2 structure possesses thermally unstable and unsaturated edges which are ready to perform in reactions; they are so called active sites. These are the locations where electrochemical processes take place, in contrast to inert basal plane unwilling to any interacting[14]. This beneficial fact, together with the instability and aggregation of few layered MoS_2 and its poor dispersibility in water[60], has let the latest research focus on the utility of 2D MoS_2 in the manner of construction of graphene hybrids. The key advantage is that combination of graphene with MoS_2 can lead to unique property arising from both building structures, which is obviously much better than their properties when used separately.

rGO/MoS_2 hybrid

Cost-effective preparation of MoS_2/graphene composite is based on liquid-phase exfoliation of bulk MoS_2 in GO solution[65]. This one-pot process of MoS_2 dispersion in GO is easy to perform and the composition of GO and MoS_2 sheets may be controlled according to their amounts used in the reaction. Nonetheless, as prepared hybrids showed layered character. Suggested schematic synthesis and structure is shown in Figure 9.

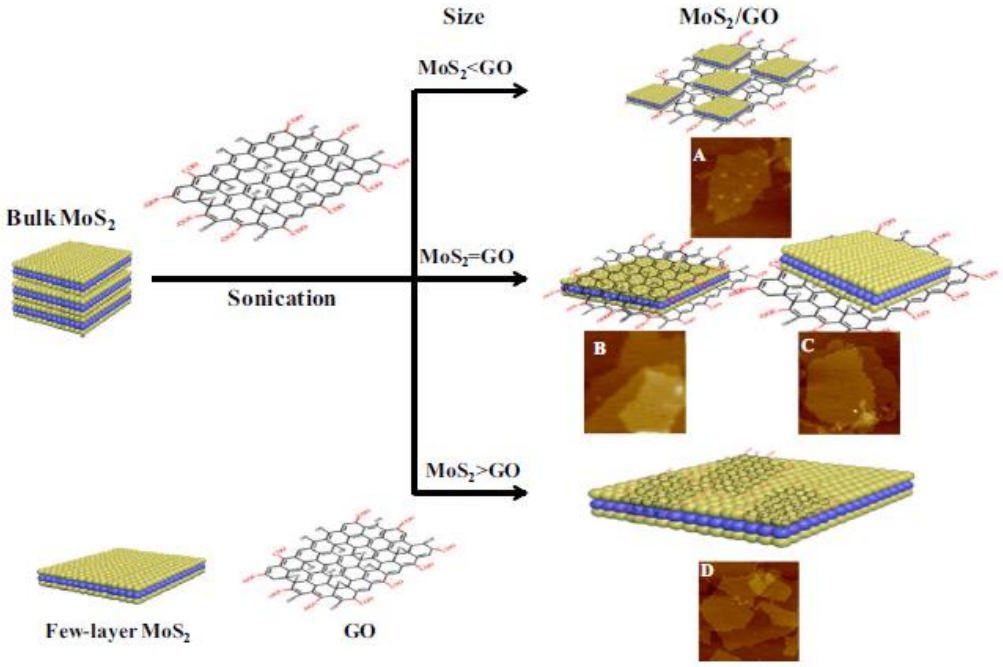

Figure 9. Scheme of liquid exfoliation process for preparation of rGO/MoS_2 hybrid. GO was used as a surfactant and its volume highly affects the final hybrid structure. [Adapted from ref. 65]

Another approach to prepare inexpensive and soluble graphene/MoS_2 composites is solvothermal reduction process, during which sulfur precursor as well as GO is reduced by reducing agent and simultaneously results in MoS_2 nanoparticles grown on rGO sheets due to thermal treatment[49,66]. Favorable is that MoS_2 nanoparticles are prevented from agglomeration due to sufficiently large GO network they are adhered to. Schematic process of the synthesis is summarized in Figure 10.

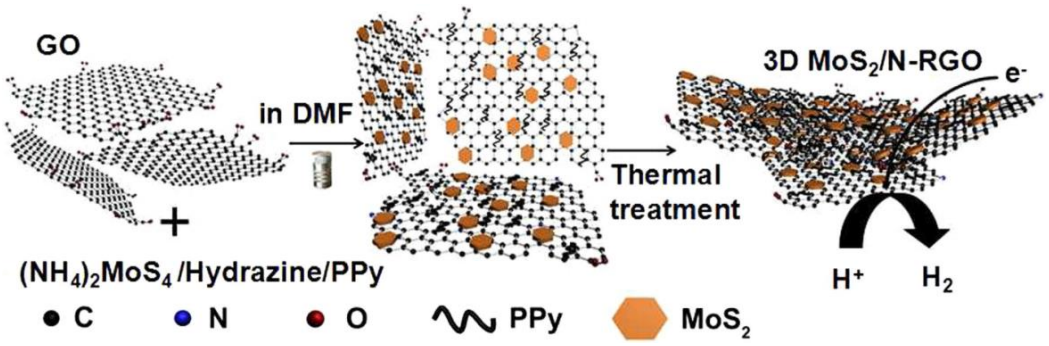

Figure 10. Scheme of reduction-solvothermal process, where MoS_2 nanoparticles are grown on GO substrate network. N-doping was performed by addition of polypyrrole. [Adapted from ref. 49]

The most suitable preparation of MoS_2/graphene composites is simple solvothermal or hydrothermal treatment reactions[12,14,55]. This process is beneficial due to one-pot self-assembling and reducing process of GO sheets and thus providing suitable conductive substrate for growth of strongly bonded 3D MoS_2 nanostructures. This hybrid structure provides the essential anti-stacking prevention, enlarges the specific surface area and facilitates access to the most amounts of active sites for both rGO and MoS_2 sheets[12,14,55]. Additionally, one-step preparation yields soluble products. Different MoS_2 precursors may be used to mix with GO dispersions, for example $Na_2Mo_4 \cdot H_2O$ with NH_2CSNH_2[12] or L-cysteine[55] and $[(NH)_6Mo_7O_{24} \cdot 4H_2O]$ with S powder[14].

In this work, rGO/MoS_2 hybrid was prepared by solvothermal synthesis according to ref. 14, consequently used for characterization, testing and understanding its structural and electrochemical performances.

6. Experiments

Materials

All chemical reagents used in this work were of analytical grade.

6.1. Methods of syntheses

Graphene oxide

The process of fabrication followed the Hummer´s method, consisting of oxidation of graphite in acidic environment[67].

In a typical process, graphite flakes (2 g, 1 wt. equiv.) was mixed with $NaNO_3$ (1 g, 0.5 wt. equiv.). Into this mixture, concentrated H_2SO_4 (46 mL) was added. Consequently, $KMnO_4$ (6 g, 3 wt. equiv.) was slowly added producing exothermic reaction. During the addition, ice bath was used to keep the temperature below 20 °C. After addition of $KMnO_4$ oil bath was used for warming the reaction mixture to 35 °C and stirred for 30 min. Then, DI water (92 mL) was added in small portions to keep the temperature of this exothermic reaction under 98 °C. Temperature of 98 °C was maintained by external heating for 15 min. After short cooling in water bath, DI water (200 mL) and 30% H_2O_2 (2 mL) were added into the reaction mixture, producing the last exothermic reaction. The reaction mixture was air cooled and stirred overnight. Then, the as prepared mixture was collected by centrifugation. Final purification started with addition of HCl (2 mL) for dissolving the metallic residues, inherited from addition of $KMnO_4$ and followed by several times centrifugation washing with DI water, neutralizing the acidic environment form H_2SO_4. Furthermore, ethanol was used, to dissolve the rest of the residues and as preparation for vacuum drying at 60 °C overnight. The as prepared GO solid phase (3.69 g) was removed from the oven and after air cooling was grinded to obtain a fine powder.

Reduced graphene oxide hydrogels and aerogels

rGO hydrogel was prepared from GO by hydrothermal reaction and freeze-dried to produce porous aerogel[13].

Typically, GO (68 mg) was dispersed in DI water (34 mL) and exposed to ultrasound for 45 min, with temperature maintained up to 35 °C, to obtain clear dispersion. As final step, this mixture was transferred into a Teflon autoclave with a volume of 40 mL, and placed into an oven for 180 °C for 12 h. By hydrothermal treatment, GO was reduced to rGO hydrogel form. Removed product was then immersed in liquid nitrogen and freeze-dried overnight to produce reduced GO aerogel with even higher porous structure and volume density (26.6 mg).

Nitrogen doped rGO hydrogels and aerogels

Graphene oxide was modified by intercalation of nitrogen atoms using hydrothermal reaction. The material used for doping was ethylenediamine (EDA)[13]. Following freeze-drying was applied to obtain porous aerogel.

Typically, GO (68 mg) was dispersed in DI water (34 mL) and exposed to ultrasound for 45 min, with temperature maintained up to 35 °C, to obtain clear dispersion. After that, ethylenediamine (200 μL) was added. As final step, this mixture was transferred into a Teflon autoclave with a volume of 40 mL, and placed into an oven for 180 °C for 12 h. Removed product was then immersed in liquid nitrogen and freeze-dried overnight to produce nitrogen doped GO aerogel with high porous structure and volume density (40 mg). The obtained sample is referred as rGO-N.

rGO/MoS_2 hybrid

rGO/MoS_2 nanohybrid was produced by solution reaction where assemblies of MoS_2 layers shaped into 3D nanostructures were formed, cross-linked with the rGO sheets[14].

Firstly, GO (84 mg) was dispersed in ethanol (27 mL) and exposed to ultrasound for 90 min. The color changed from black to brown during the dispersion process. Meanwhile, S powder (0.077 g) was dissolved properly in octylamine (28 mL) and ammonium molybdate tetra hydrate [$(NH_4)_6Mo_7O_{24} \cdot 4H_2O$] (0.093 g) was added. Then the as prepared mixture was added into GO dispersion and put in ultrasound bath for another 5 min. Finally, the reaction mixture was transferred into a Teflon autoclave with a volume of 70 mL and placed into an oven set up to 200 °C for 6 h. After air cooling, the product was removed and purified several times with ethanol in centrifuge. After purification, the product was vacuum dried at 60 °C overnight (1.5 mg). This is referred as rGO/MoS_2.

7. Results and discussion

Characterization

All samples were examined and characterized by following techniques. Here is short introduction to their principals. X-ray diffraction (XRD), a crystallographic method applying X-ray beams to the crystal to collide with intrinsic atoms and analyses its interference with elastic scattering of crystal electrons. In resulting diffraction pattern can be found information about crystal order/disorder, interlayer spacing and atomic position. Scanning electron microscopy (SEM), which is special kind of microscope imaging in which the materials surface is bombarded by focused beam of electrons and is analyzed by characteristic responses of such generated secondary generated electrons. Transmission electron microscopy (TEM) is imaging of materials surface using highly accelerated electrons to pass through the sample and their focusing on detector display. Energy dispersive X-ray analysis (EDS) is elemental analysis technique which detects small X-ray emission of particular elements caused by electron bombarding in SEM and analyzes the presence and amount of elements[76]. CHNS analysis is another elemental analysis facilitated mainly to determine the presence of C, N, H, and S, where sample is combusted and generated gases are separated accordingly to elemental composition[77]. Raman spectroscopy is typical characterization method regarding carbon materials. It is nondestructive method for analysis of spatial arrangement of the sample´s molecules and order/disorder of the crystal lattice. Such information is analyzed from inelastic Raman scattering with characteristic wavelength for every molecule generated as pulse laser is applied on the sample. For graphene, there are special signs including D band, which is used to describe the degree of disorder and defects within the sp^2 graphitic plane by forming sp^3 distortions and G band, which is represented by sp^2 carbon domains and is sensitive to number of layers and therefore doping[18,63]. Fourier transform infra-red spectroscopy (FTIR) is method in which infra-red radiation is applied on sample and generated vibrational modes (characteristic for each bond) are detected on thermal/electric detector. Such method is usually carried out to identify the chemical structure of the sample and to accompany Raman analysis. Fourier transformation is used to obtain targeted amplified spectrum. X-ray photoelectron spectroscopy (XPS) is non-optical technique based on detecting of electrons emitted from the sample as a response to application of high energy X-

ray radiation. This technique is used for identification of intrinsic binding energies in excited state, qualifying and quantifying presented chemical bonds[75].

Further evaluation included electrochemical characterization by cyclic voltammetry (CV) and electrochemical impedance spectroscopy (EIS), which will be described further in the text. Whereas the spectroscopy analyses were performed mostly in a solid phase and served for description and understanding the formation process and structure of the composite, for electrochemical evaluation was used aqueous dispersion.

7.1. Spectroscopy and microscopy analysis

7.1.1. Graphene oxide (GO)

GO is firstly described as the starting material for further functionalization in order to compare and comprehensively understand the nature of N-doped rGO. The structure, content and morphology change of the GO sheet with respect to graphite may be seen in SEM, XRD, Raman and FTIR image in Figure 11 a, b, c and d. SEM evaluates GO as layered material with non-uniform thickness of stacked layers (Figure 11a). FTIR verifies the increment of oxygen functionalities during the conversion process (Figure 11b). There are hydroxyl groups (3411 cm^{-1}) as the major representative and C=C bond which is obviously caused by successful exfoliation of graphite aromatic layers. Further oxygen signals prove addition of ketone, epoxy and C-O vibrations modes in contrast to graphite[32]. EDS analysis for atomic representation was carried out during SEM analysis which shows carbon, oxygen and sulfur elements in decreasing manner. Low but considerable sulfur detection limit is therefore potential proof of residual sulfate linking from H_2SO_4 intercalation during the first step of the synthesis.

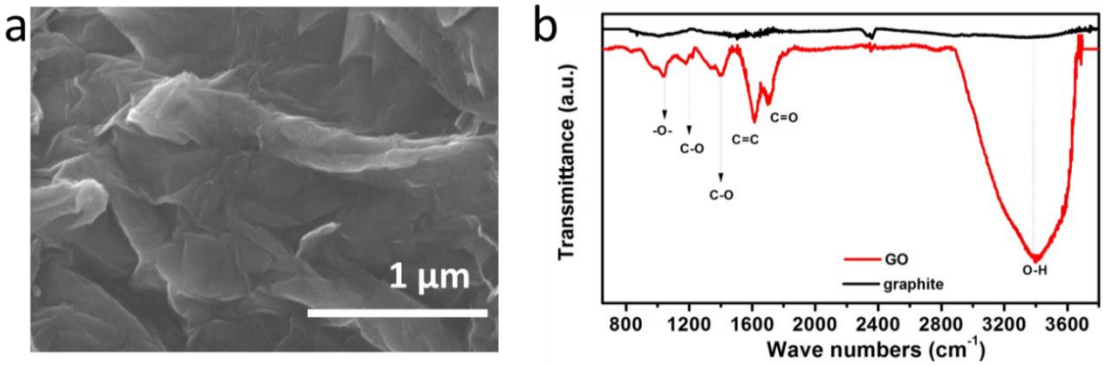

Figure 11a-b. a) SEM images of GO; b) FTIR spectrum of GO sample.

XRD diffraction peak at 2θ=31° corresponds to the graphitic structure (Figure 11c) with a d-spacing about 3.4 Å [68,69]. Process of functionalization of graphitic network is therefore proved, since this peak disappears in GO. Instead, new peak at 2θ=13.1° is created, which indicates typical diffraction peak of GO resulting from sp^3-like defects in sp^2 aromatic network caused by extension attachment of oxygen functionalities on the GO surface and expansion of graphitic layers[19,70]. The d-spacing at this peak is 7.87 Å indicating successful attachment of oxygen functionalities to GO surface. The broadness may suggest amorphous character of GO. Clear evidence of significant increment in graphitic sp^3 hybridization in GO shows typical G and D bands of Raman analysis (Figure 11d) The G band of at 1580 cm^{-1} indicates the same position for graphite and GO since this is sign of hexagonal sp^2 carbon network in GO sample. D band at 1350 cm^{-1} hence relates to oxygen groups on GO. The relation of D/G band intensities is more illustrative way for comparison; we may say that according to I_D/I_G ratio of GO (0.96), there is sp^2 hybridization present in the majority over the sp^3 carbon atoms, despite of the damaged aromatic network[71]. In comparison with graphite that shows sharper G band and lower I_D/I_G ratio (0.42), it is easy to assume significantly lower disruption of aromaticity in case of graphite and high degree of oxidation in GO.

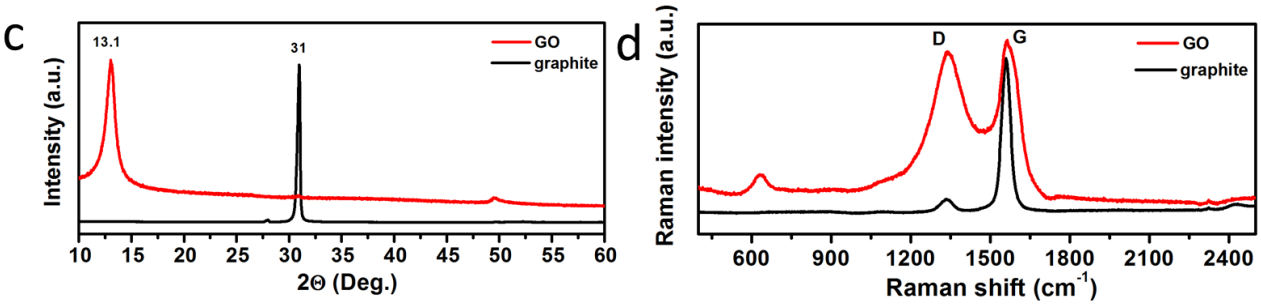

Figure 11c-d. c) XRD patterns of GO and graphite; d) Raman spectra of GO in comparison to graphite.

7.1.2. Nitrogen doped reduced graphene oxide (rGO-N)

GO is the starting material, into which EDA is intercalated during hydrothermal reaction to play a role as a source of nitrogen, as well as the modifier of the inner structure of the product[13]. As a control experiment we synthetized undoped rGO for comparison. Also, rGO-N aerogel was prepared by freeze-drying method with pre-freezing in liquid nitrogen. CHNS analysis was carried out to determine the elemental quantification of rGO-N and results indicate C, N and H percentage as following: C: 67%, N: 11%, H: 20% (at%), respectively.

The morphological features of rGO-N sample is shown in SEM images in Figure 12a and b. SEM image of rGO-N showed organized porous structure. Liquid nitrogen keeps the temperature under-freezing point of water and so the ice crystals in the pores may growth enough to force towards the GO sheets and make them more stacked and restored in favor of denser pore network. The characteristic layered and transparent nature of graphene is clearly seen from SEM images.

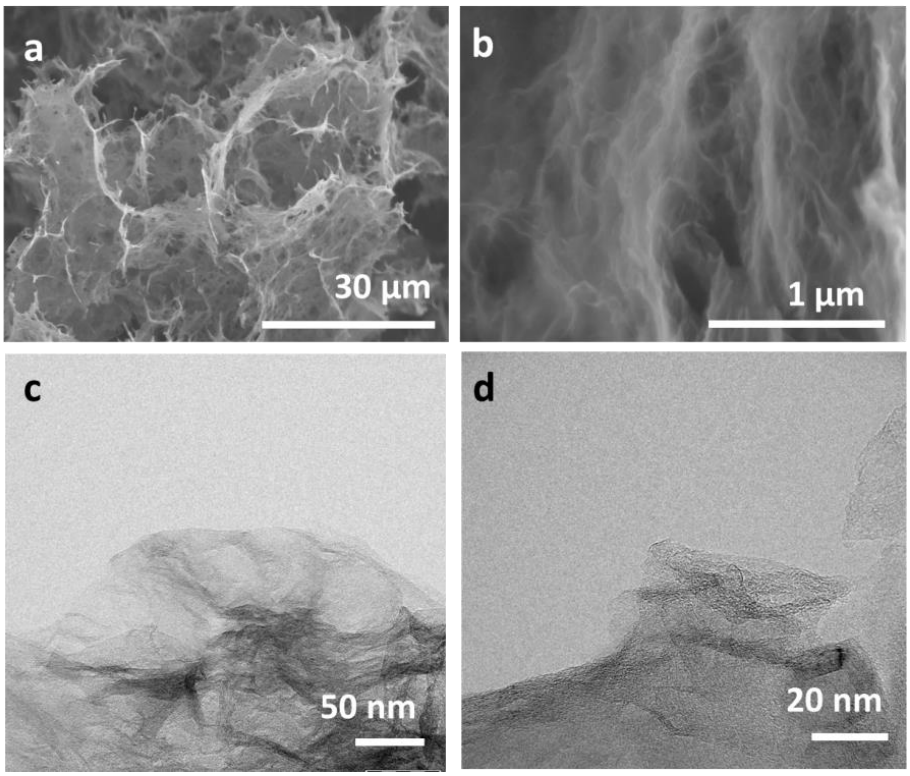

Figure 12. a,b) SEM images of rGO-N; c,d) TEM images of rGO-N sample showing distinguishable edge layers.

TEM images signify the transparent and homogenous layered structure of rGO-N and also prove that GO sheets are stacked into few-layered structure. Their overlapping and folded edges are seen in Figure 12 c,d. This is a confirmation of wrinkled and variably shaped edges typically observed in graphene finite-size sheet[71] and they may be considered as the starting positions of EDA attack on GO.

Process of oxidation and intercalation is usually monitored by XRD reflection patterns. As previously mentioned, reduction of graphite is typically observed due to missing of its strong peak at 2θ=31° and its functionalization to GO is observed due to new peak appearance at 2θ=13.1°. Figure 13a shows, that oxygen groups on GO are reduced by the EDA interaction because GO´s peak at 2θ=13.1° is not observed after the hydrothermal

reduction. Broader and down-shifted graphitic peak is however presented in rGO-N at 2θ=28.4°, as well as in undoped rGO, signifying d-spacing of 3.6465 Å and 3.6463 Å for rGO-N and rGO, respectively. This however confirms, that no special extension of rGO sheets occurred during EDA doping, which is in agreement with other reports[68,69] and ascribed to the not sufficient size of EDA to intercalate properly and indicating rather stitching the rGO sheets. The same positions of the peak for doped and undoped rGO confirm the reduction of oxygen species from GO surface. Meanwhile, the exact determination of EDA´s reduction performance though verifies the comparison of the intensities of graphitic peak at 2θ=28.4°[,69].

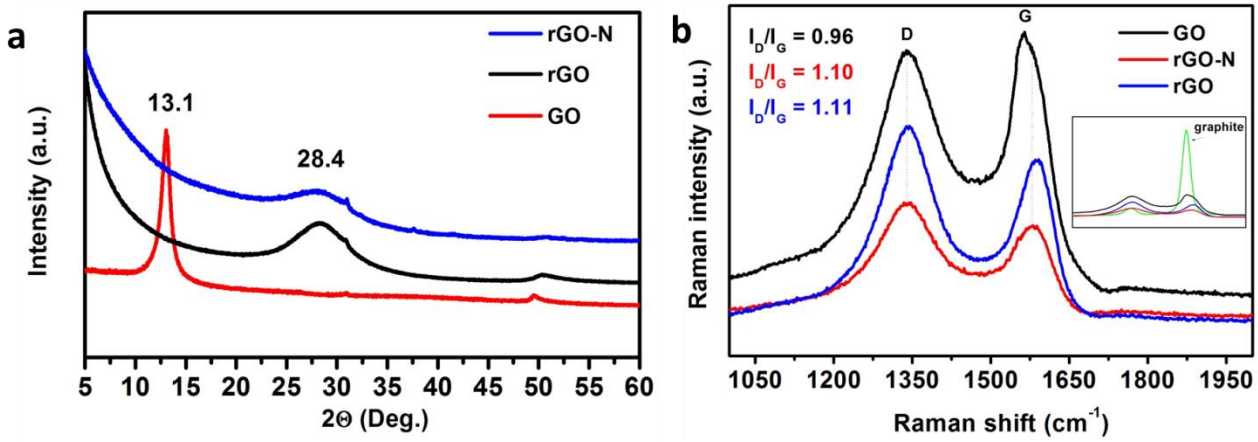

Figure 13. a) XRD patterns of rGO-N sample in comparison with rGO and GO; b) Raman spectrum of G and D bands of rGO-N sample in comparison to rGO and GO. For illustration, the inset shows the G band of precursor graphitic peak.

Raman analysis was examined in order to further compare the carbon configuration and hybridization in our sample. According to analyzed G and D band in Figure 13b there is trend change from GO to rGO and rGO-N. While the D band remains in approximately same position for all samples, the G band is different for each sample. Additionally, I_D/I_G ratio differs for each sample indicating both modified samples damage the sp^2 network. Increment in I_D/I_G ratio of rGO in contrast to GO and upper shift of the G band is attributed to introduction of oxygen species on GO surface and reducing of graphitic domains[29]. Higher I_D/I_G ratio of rGO-N (1.10) with respect to GO (0.96) and upper shift of G band confirms the restoration of graphitic sp^2 sheets as a result of N functionalization, which agrees with the previous studies[69,72]. However, the upper G band shift in case of rGO with respect to GO was unexpected since simple reduction reactions of GO were observed in downshift of the G

band[29,68,69]. Recent studies also propose that EDA reduces the crystallite size (L_a)[69], which was confirmed in our samples by calculation from the equation [1][52].

$$L_a(nm) = (2.4 \cdot 10^{-10})\ \lambda^4\ (I_D/I_G)^{-1} \quad (1)$$

where λ^4 is the laser excitation wavelength.

L_a drops from 16.69 nm in GO to 14.31 nm in rGO and 14.56 nm in rGO-N. This may explain how both amine-terminated EDA edges stitches the neighboring rGO sheets together[68], in other words it corresponds to the I_D/I_G ratios in the graphs. The more close or stacked the layers will be the lower crystals will be formed.

In order to understand the nitrogen bonding and functionalities in the rGO-N sample we investigated the FTIR and XPS spectra, which are summarized in Figure 14 and 15. According to changes in molecules bond vibrations in Figure 14, EDA interacts with carboxyl, epoxy and alkoxy groups on the GO surface. Reduction of carboxyl groups in rGO may be seen in noisy disappearing of C=O vibrations and noisy downshift in C=C vibrations in rGO. Otherwise, broad peak ranging from 1515 to 1560 cm^{-1} in rGO-N indicates that carboxyl groups were further functionalized forming C-N vibrations, which suggest formation of amide bond. Epoxy and alkoxy groups in central GO plane show one condensed broad peak in case of rGO also indicating their reduction. In case of rGO-N they further interact with EDA and form even broader peak of amine bond vibration.

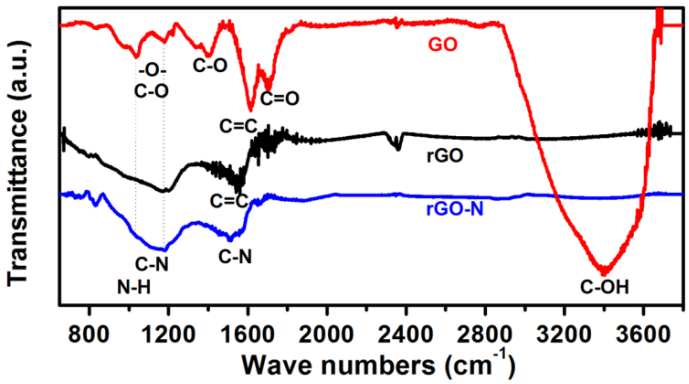

Figure 14. FTIR spectrum of rGO-N sample compared to rGO and GO.

XPS analysis in Figure 15a, b and c shows C 1s, N 1s and O 1s spectra of rGO-N sample respectively. Carbon bonding verifies the highest representation of sp^2 carbon network, significant contribution of its defects by sp^3 binging energy, presence of alkoxy

groups remained after reduction reaction of EDA which is in agreement with theory which states that complete removing of oxygen functionalities by reduction is impossible. Finally, determined C=O peak in the C 1s spectrum signifies that carboxyl groups were neither completely reduced. Nevertheless, carboxylic percentage is the lowest, which is agreement with their edged-location and thus first groups to be reduced in EDA presence. N 1s spectrum confirms three N configurations with the highest percentage of pyrrolic N, followed by pyridinic type and the lowest percentage is represented by graphitic N. This reveals that the main kind of doping corresponds to in-plane in-ring substituted nitrogen. Oxygen 1s spectrum only verifies the incomplete reduction of carboxyl and alkoxy groups. Supplementary EDS (Figure 15d) evaluates the main atomic composition of carbon, oxygen and nitrogen indicating successful doping of GO by nitrogen. However, overall elemental analysis evaluated by XPS for C, N and O are 94.3%, 8.7% and 6.8% (at. %) respectively.

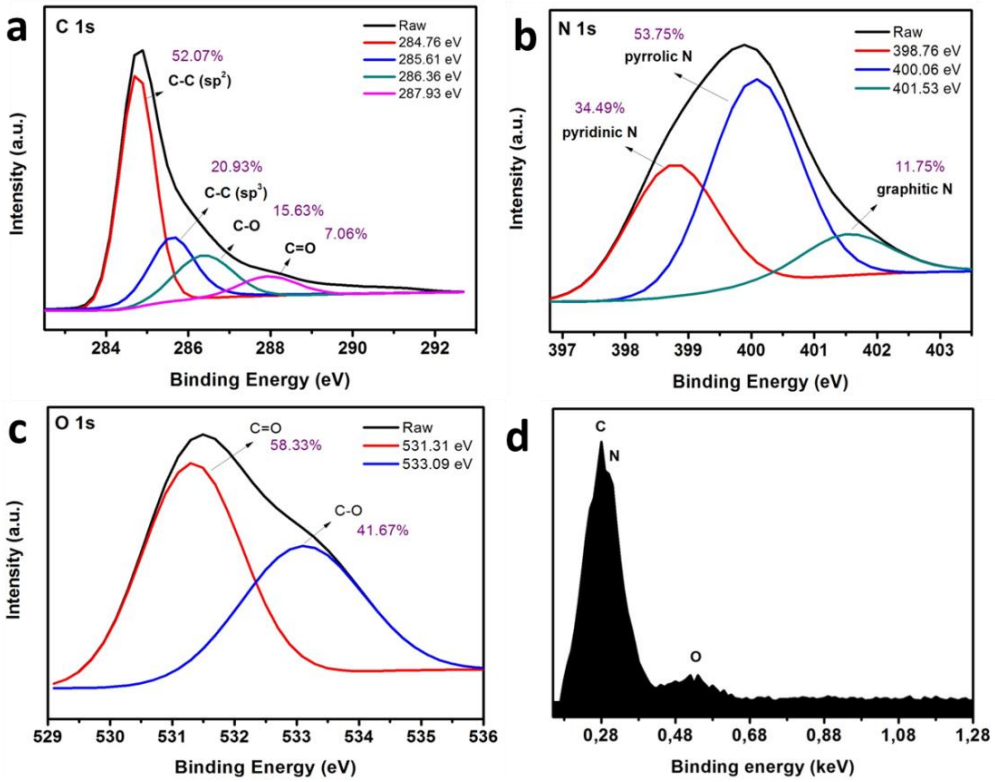

Figure 15. XPS spectra of rGO-N sample. a) Deconvoluted high resolution C 1s spectrum, b)N 1s spectrum, c) O 1s spectrum, d) EDS of the rGO-N sample.

In summary, few-layered porous rGO-N were prepared by freeze casting of nitrogen functionalized rGO hydrogel. Immersion into liquid nitrogen before freezing process resulted in lower weight of the aerogel and successful exfoliation, oxidation and functionalization of GO was confirmed by XRD. XPS spectra indicate the structure of rGO-N is composed of

pyridinic, pyrrolic and graphite type N bonding. Successful functionalization by EDA was finally confirmed by elemental analysis with nitrogen content of 8.7 at%.

7.1.3. Reduced graphene oxide/MoS_2 hybrids

GO, ammonium molybdate and sulfur powder were the starting materials for the preparation of rGO/MoS_2 hybrids. The formation of the hybrid was carried out in under solvothermal conditions, where ethanol is used as a solvent and octylamine as MoS_2 surface ligand[14].

SEM imaging was performed to see the morphological constitution of the hybrid assembly and results are shown in the Figure 16a and b. Indeed images clearly indicate combination of 3D nanostructures of MoS_2 in size of hundreds of nanometers, on crumbled 2D-rGO sheets, which act as a support maintaining the stability of the hybrid. This assembly is ascribed to the solvothermal reaction conditions[14]. EDS in Figure 16e confirms the presence of C, Mo and S in the hybrid. According to detailed TEM microscopy images (Fig. 16c,d) we observe that the 3D assembly consisting of wrinkled layered composition. Magnification of the rGO/MoS_2 in Figure 16d reveals layered composition on the edge sites.

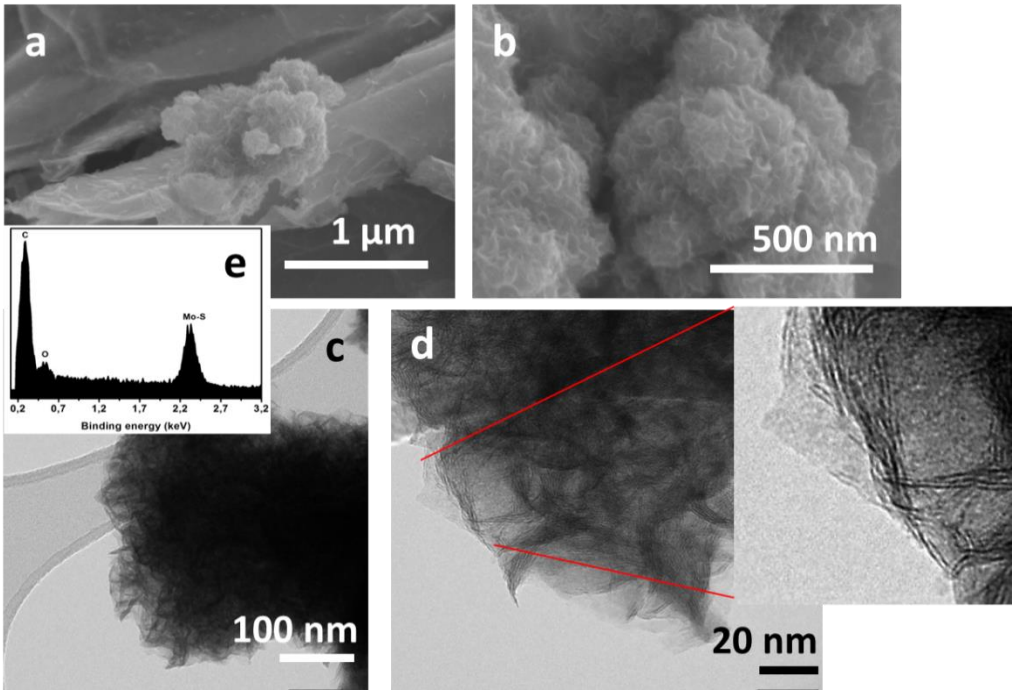

Figure 16. a-b) SEM images of macroscopic and sub-microscopic rGO/MoS_2 hybrid structure, c-d) TEM images of rGO/MoS_2 hybrid, e) EDS of rGO/MoS_2 sample.

XRD analysis was evaluated in order to identify the crystallite structure of rGO/MoS_2. In Figure 17, there is diffraction pattern of rGO/MoS_2 and GO in comparison, showing that

the MoS_2 crystallites influence the pattern with broader and less intense peaks in contrast to GO[14,66]. The hybrid possesses typical graphitic peak at 2θ=27.5° (2θ=31° for pristine graphite). This suggests that oxygen species of GO are reduced in hybrid in favor of renewed graphitic carbon. Relatively small peak at 2θ=13.7° likely represents residual GO pattern (2θ=13.1°), however it can be considered as a MoS_2 crystal pattern as well[12,14]. The other peaks of MoS_2 crystal formation are observed at 2θ=38.6° and 2θ=50°,[14,49,55,66]. The second peak can be analogously considered as graphitic framework network [70], similarly to residual peak at 2θ=42° in case of GO.

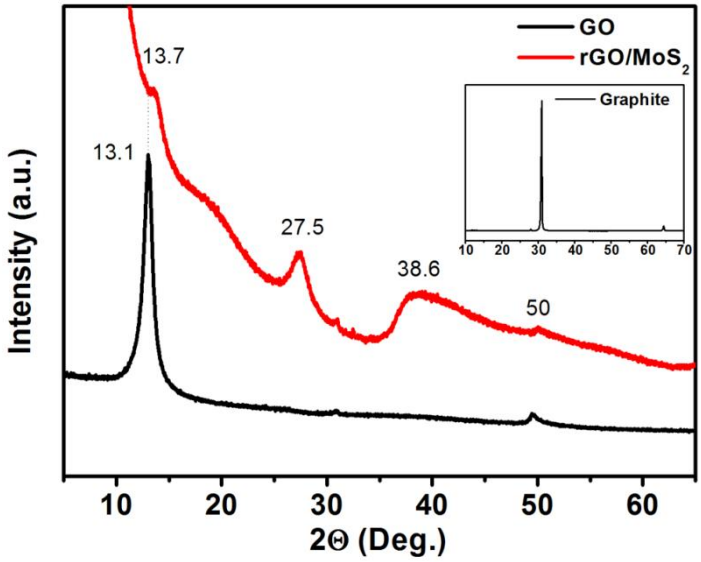

Figure 17. XRD patterns of rGO/MoS_2 sample in comparison with GO as starting material.

Raman analysis reveals the differences in sp^2 structure in the process of GO reduction and growth of MoS_2 clusters (Figure 18). G and D bands, characteristic for GO are observed in spectrum. Interestingly, the upper shift of G band goes from GO (1560 cm^{-1}) to rGO/MoS_2 (1588 cm^{-1}) which, according to the original study[14] should be represented by downshift as a reflection of N heteroatom presence (from octylamine or even ammonium molybdate precursor). Thus, in case of rGO/MoS_2 hybrid, octylamine or residual ammonium can be possibly considered as very weak functionalization of oxygen species too. Additionally, the I_D/I_G ratio increases from GO (0.96) to rGO/MoS_2 (1.10), which corresponds to the process of converting of GO sheets, as they are suffering from sp^2 lattice disordering caused by MoS_2 nanostructure growth. Obvious presence of MoS_2 composition can be found in peaks ranging from approximately 100 to 1000 cm^{-1},[14]. O-Mo-O vibration modes are detected around 345 cm^{-1}, indicating oxidation of Mo-S bonds and significant 809 cm^{-1} and 985 cm^{-1} peaks signifies the Mo=O vibrations of MoO_3 band[73], most likely formed by the reduction of

ammonium molybdate precursor. Raman shift at 650 cm^{-1} was attributed to another characteristic peak of MoS_2 crystal[71,73].

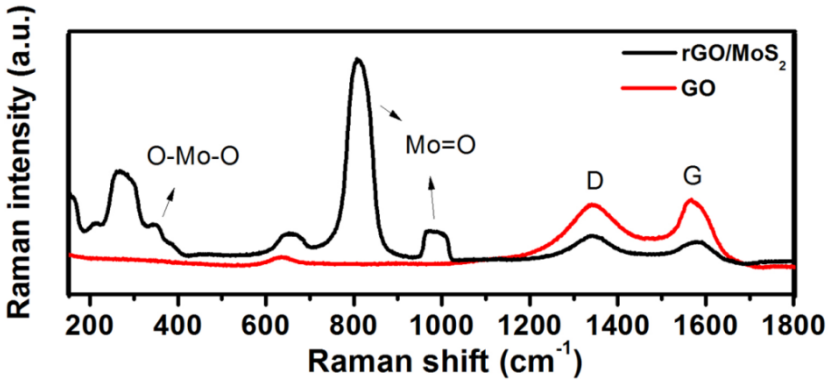

Figure 18. Raman spectrum of rGO/MoS_2 sample with respect to GO.

FTIR analysis reveals the bonding formation between rGO and MoS_2 nanostructures (Figure 19). rGO/MoS_2 hybrid possesses significantly reduced intensities of characteristic GO vibrations indicating the reaction between GO and MoS_2 precursors and resulting reduction of oxygen species [12,14]. Characteristic -CH_2 and -CH_3 vibrations together with N-H modes around 1445-1530 cm^{-1} determine the presence of surface ligand -octylamine, which constrains the MoS_2 assembling and growth on the GO active sites[14]. The peak at 938 cm^{-1} suggests that reduced oxygen groups are simultaneously coupled into Mo-O-C bonds with MoS_2 precursor[55]. Thus, Mo is attached most likely *via* epoxy-, alkoxy-, and hydroxyl-groups, whose reduction is most significant. Moreover, insignificant but considerable downshift at the O-H vibrations in rGO/MoS_2 sample (from 3402 cm^{-1} in GO to 3379 cm^{-1} in rGO/MoS_2) may indicate participation of sulfur as hydrogen bonding acceptor[74]. In this point of view, O-H groups are also suggested to interact with S and form S···H-O hydrogen bonds.

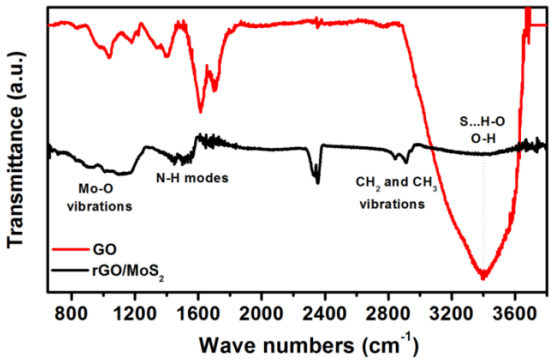

Figure 19. FTIR spectra of rGO/MoS_2 and GO.

XPS characterization of the components of rGO/MoS_2 hybrid is summarized in Figure 20. High resolution spectrum of C 1s (Figure 20a) only verifies the minimalized content of surface oxygen groups and O 1s spectrum (Figure 20b) further specifies that main oxygen bond in formed with Mo (C-O-Mo)[55], which agrees with previous FTIR results. MoS_2 is characterized in Figure 20c by Mo 3d high resolution spectrum indicating the presence of Mo $3d_{(5/2)}$ and Mo $3d_{(3/2)}$ as the main contributors of Mo^{4+} configuration[14,49,55]. MoO_3 formation (Mo^{6+}) from ammonium molybdate precursor is reduced by original oxygen coated GO surface in favor of Mo^{4+} and Mo^{5+}[,49,66]. Finally, Mo 3d spectrum defines also S 2s resolution spectrum which after deconvolution (Figure 20d) reveals the S $2p_{(3/2)}$ and S $2p_{(1/2)}$ sulfur modes occupying the highest percentage. Importantly, S^{-2} unaffected configurations are defined in raw S 2p spectrum in higher binding energies (169 eV) which were proved as the active sites for electron transfer between the GO sheets[12]. XPS elementally analysis revealed the presence of C, S, O and Mo atoms in 66.3%, 16.5%, 9.4% and 7% (at. %) representation, respectively.

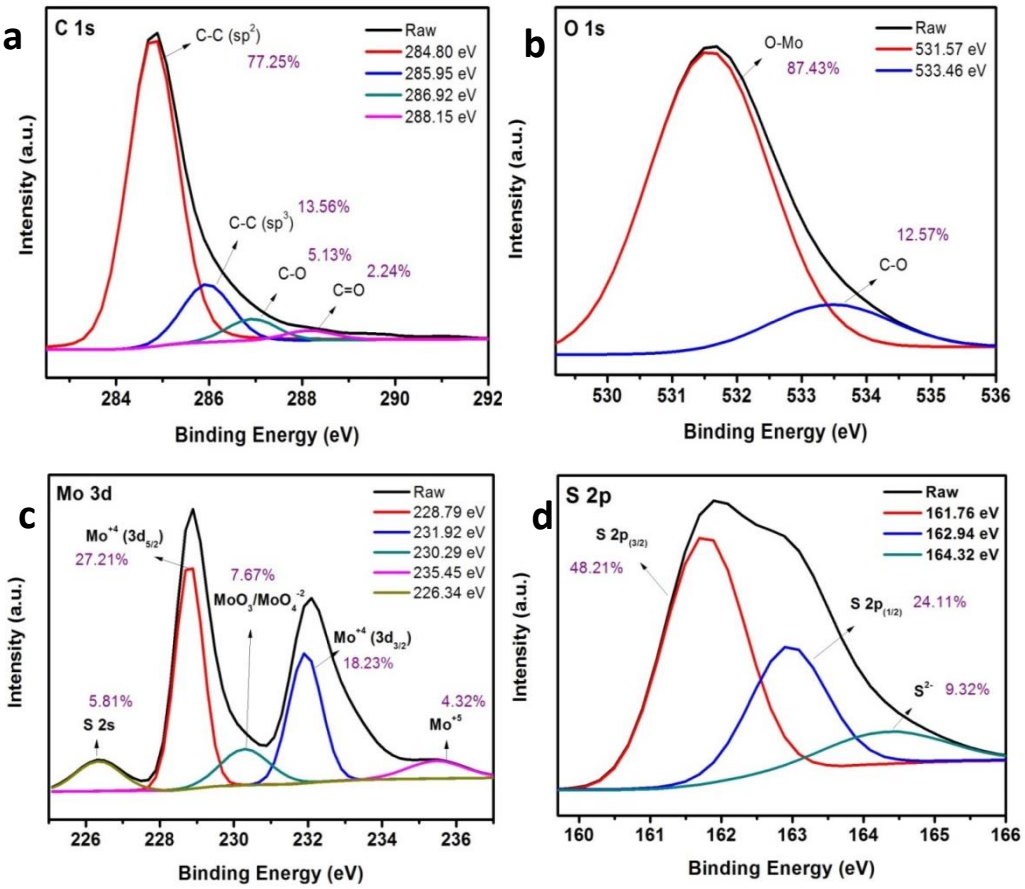

Figure 20. XPS analysis of rGO/MoS_2 sample. Deconvoluted high resolution spectra of: a) C 1s spectrum; b) O 1s spectrum; c) Mo 3d spectrum; d) S 2s spectrum.

In conclusion, we synthesized and characterized rGO/MoS_2 hybrid as following: reduction of GO, confirmed by XRD, Raman and FTIR analysis is attributed to solvothermal conditions and mutual interaction with ammonium molybdate. MoS_2 composition is confirmed by XPS analysis indicating the Mo:S ratio as 7:16 along with the presence of unsaturated sulfide active sites. Presence of MoS_2 clusters on the rGO is verified by microscopic techniques. Furthermore the attachment to rGO further indicated by the FTIR and XPS results showing C-O-Mo bonding.

The 3D interconnected network based on rGO nanostructures (rGO-N and rGO/MoS_2) and its electro-active functionalization makes both graphene-based materials well equipped for electrochemical performance when used for electrode modification. In case of rGO-N free electron pairs originated from nitrogen in the graphene framework catalyzes the oxidation activity. However for rGO/MoS_2 hybrid, conductivity of rGO is supported most likely *via* H bonding that fastens negatively charged MoS_2 nanosheets. Furthermore, extensive porous structure of rGO-N and constitution of 3D MoS_2 nanosheets can provide higher area where redox reaction can take place and thus enhance overall electrochemical performance. This motivated us to utilize rGO hybrid nanostructures for electrochemical applications.

7.2. Electrochemical characterization

Electrochemistry is a discipline that deals with chemical reactions that involve an exchange of electric charges between two substances. Both, chemical changes generating electric currents and chemical reaction caused by the passage of electricity can be considered as electrochemical reaction occurring at the electrode/electrolyte interface. Such changes are generally known as redox reactions, during which the charge flows simultaneously from negative to positive substance and results in one substance oxidized and one reduced.

The most common set-up used for electroanalytical measurements consists of three electrode system including working electrode (WE), reference electrode (RE) and counter electrode (CE) connected to a potentiostat. In this case, the current flows between the CE and WE. The potential difference is controlled between the WE and the CE and measured between the RE and the WE. The potential between the WE and CE is not usually measured. The working electrode is the electrode on which the reaction of interest is occurring and commonly is made of inert materials such as gold, platinum, silver, glassy carbon or mercury.

The reference electrode is an electrode which has a stable and well-known electrode potential and it is used as a point of reference in the electrochemical cell as already mentioned above. For this purpose, saturated calomel or silver/silver chloride electrodes are employed. The counter electrode (also known as auxiliary electrode), is an electrode which is used to close the current circuit in the electrochemical cell. It is usually made of platinum, graphite or other carbon material and usually it does not participate in the electrochemical reaction.

Cyclic voltammetry and electrochemical impedance spectroscopy are electroanalytical techniques usually used as first methods for basic electrochemical characterization of studied system. In the case of cyclic voltammetry (CV), a potentiostat is employed to apply voltage into the electrochemical cell to induce redox reactions and subsequently generated Faradaic current is measured. As an output cyclic voltammogram, in which current is plotted against the voltage applied to an electrochemical cell is obtained. Despite voltage can be applied with different scan rates, it is always applied linearly with time dividing one cycle into forward scan (increasing of applied potential) and reverse scan (decreasing of applied potential). Oxidation and reduction peak heights (maximal anodic and cathodic currents) quantify the amount of analyte oxidized/reduced on the electrode surface, while the peaks position defines them qualitatively[64].

From the overall shape of cyclic voltammograms one can also deduce on quality of electron transfer kinetics of studied redox system. CV voltammogram provides very important identification about the reversibility of particular redox reaction associated with Nernst and Randels – Sevcik equations[64]. As the reversible/irreversible behavior of the redox system arising from thermodynamical equilibrium it can be well described according to Nernst equation [2]. Generally, the peak potential should be independent on scan rate and equal to each other. The difference between potentials of anodic and cathodic current (peak to peak separation of half reactions, Epa – Epc) for fully reversible behavior should indicate $59\ \mathrm{mV}\cdot z^{-1}$ as this is the constant that includes the thermodynamical parameters. Higher separation is sign of increasing system´s irreversibility[64].

$$E = E^{\circ} - \frac{RT}{zF}\ln\frac{a(red)}{a(ox)} \qquad (2)$$

where E and E° is the electrode potential and standard electrode potential, R is universal gas constant, F is Faraday constant, T is thermodynamic temperature, z is number of electrons exchanged during the reaction and a(red), a(ox) is the chemical activity of reduced and oxidized form of redox material.

The other identifications are defined by Randels – Sevcik equation [3], focusing on peak current definition. Many factors are found to influence the current response as shown in the equation, while for electrode characterization the dependence of peak current on the square root of scan rate and the area of the electrode surface are of significant importance. For obtaining the best current responses on desire electrode, the current dependence on square root of scan rate have to show linear relationship, indicating that electron transfer is diffusion controlled. The area of electrode has to be as large as possible to provide the maximal place for participating reactions.

$$I_{Pc} = I_{Pa} = 2.69 \cdot 10^5 \cdot n^{3/2} \cdot D^{1/2} \cdot v^{1/2} \cdot A \cdot C \qquad (3)$$

where n is the number of electrons transferred in one redox reaction, D is diffusion coefficient, A is the electrode area and C is concentration of redox material.

Electrochemical impedance spectroscopy (EIS) is an analogue technique which converts the resistance of measured system most commonly into Nyquist plot, illustrating capacitive and faradaic resistance of charge transfer. In general, Nyquist plot consists of semicircle whose diameter corresponds proportionally to faradaic current and of straight line indicating charge transfer resistance of redox reaction. Typically, potentiostat is used to apply alternating voltage into electrode system and obtained resistance gives information about the constitution and conductive behavior of the electrode material[14].

Materials and methods

In this work, both materials rGO-N and rGO/MoS_2 were used for the modification of glassy carbon electrodes (GCE) by drop-coating method, whose principle is illustrated in Figure 21a. Before electrode modification, water dispersion of sample (1mg ml^{-1}) was shortly sonicated and then 10 µl of dispersion was dropped onto GCE surface and allowed to dry at room temperature. Undoped rGO was also used for GCE modification as material used for blank experiments in order to see the effect of doping/functionalization. Modified electrodes were then employed as working electrode in three-electrode system including also silver/silver chloride (Ag/AgCl) as reference electrode and stainless steel wire as counter electrode (see Figure 21b). Each electrochemical measurement was performed in 0.1M KCl containing 5mM $K_4Fe(CN)_6/K_3Fe(CN)_6$ (1:1) and current responses of modified electrode were monitored by CV or EIS. All electrochemical measurements were performed using a potentiostat Autolab PGSTAT 128N.

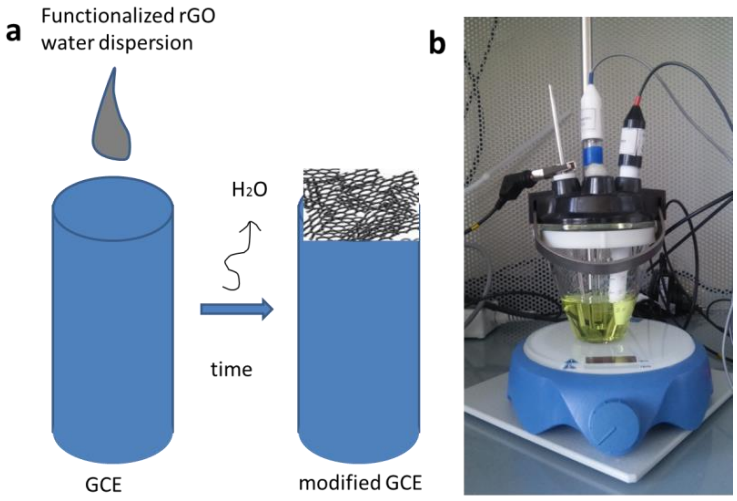

Figure 21. a) Illustration of drop-coating method used for electrode modification, b) Electrochemical cell used for all electrochemical measurements.

Results and discussion

7.2.1. N-doped reduced graphene oxide aerogel

CV measurement was performed at the scan rate of 50 mV/s with GCE modified with rGO-N and rGO as can be seen in Figure 22a.

CV voltammograms of rGO-N modified electrode compared to the GCE indicate substantial enhancement in peak current responses to redox probe. In this case, peak current observed on rGO-N electrode is more than once higher than that of unmodified electrode. On the other hand, electrode modified with rGO showed similar peak current responses as those obtained with electrode modified by rGO-N. More rectangular shape of the curve obtained with rGO modified electrode is indicator of higher capacitive current and thus higher electrode surface area when compared to rGO-N. Measurements for both modified electrodes showed stability and reproducibility, performing constant response upon 10 cycles of recording.

Kinetics of charge transfer stayed as an object of interest for following measurements. For this reason, a scan rate study for electrode modified with rGO-N was performed (Figure 22b). It was observed that peak current readily increased with increasing scan rate in the range of 10 to 150 mV s^{-1}. In Figure 22c is shown good linear relationship between the square root of scan rate and peak current, indicating that the electrode process is diffusion controlled.

As already mentioned, electron transfer properties of the system can be observed from peak to peak separation ($\Delta E = E_{pc} - E_{pa}$). Based on CV measurements depicted in Figure 22a we can demonstrate that the fastest electron transfer was performed on bare GCE. However, when comparing modified electrodes, rGO-N modified electrode performed faster electron transfer and therefore better reversibility of the reactions occurring on the electrode/electrolyte interface in contrast to GCE modified with undoped rGO according to lower peaks separation. Calculated values of peak to peak separation for all three electrodes are summarized in Table 1.

Table 1. Table of ΔE values for two differently modified GCE electrodes and value for GCE.

electrode	E_{pa} - E_{pc} (mV)
GCE	120
GCE + rGO	139
GCE + rGO-N	130

The electron transfer properties were further characterized by electrochemical impedance spectroscopy as can be seen in Figure22d. Nyquist plot illustrates how porous architectures represented by rGO and rGO-N aerogels contribute to higher capacitive current and thus enable faster electron transfer having almost no resistance. Faradaic semicircle of both modified electrodes is incomparably lower than that of GCE and sharply increasing line of charge diffusion resistance is a sign of advanced electron transfer in modified electrodes. Slightly less steep growing for rGO-N with respect to rGO is identification of lower capacitive character.

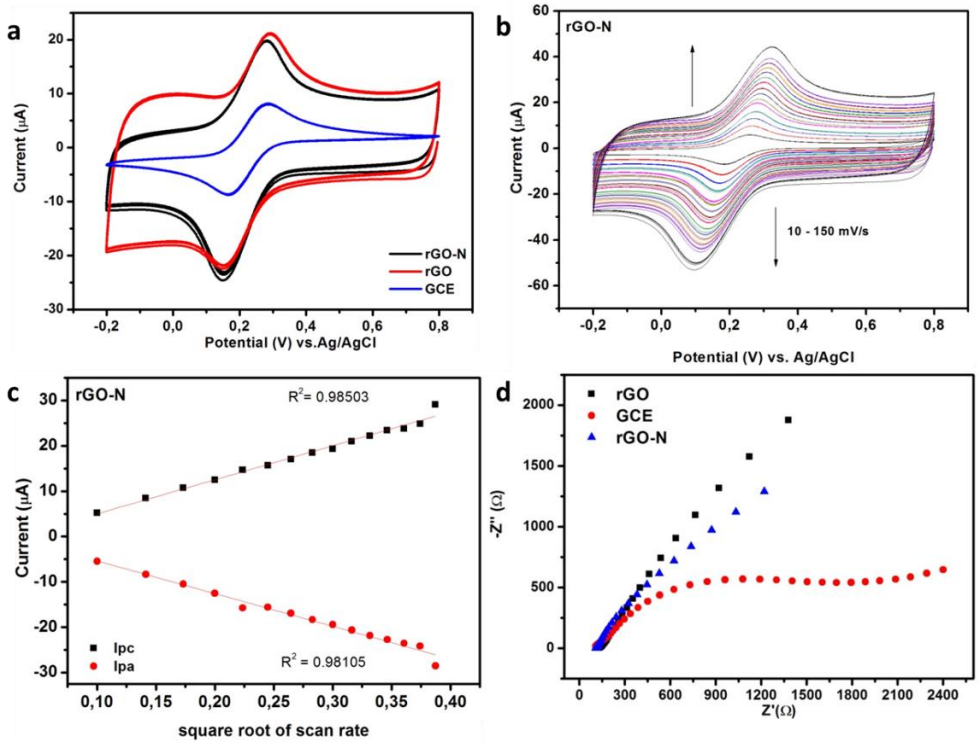

Figure 22. a) Cyclic voltammograms recorded by unmodified GCE and GCE modified with rGO or rGO-N. b) CV voltammograms recorded with GCE modified by sample rGO-N at different scan rates (10 to 150 mV/s), c) Plot of anodic and cathodic currents vs. square root of scan rate measured by GCE modified with rGO-N, d) EIS measurements for rGO-N modified electrode with respect to GCE modified with rGO and bare GCE.

7.2.2. Reduced graphene oxide/MoS_2 hybrids

Electrochemical activity of rGO/MoS_2 was evaluated with respect to bare GCE in the same conditions as previous measurements and overall characterization can be seen in Figure 23.

CV voltammograms of rGO/MoS_2 hybrid as surface modification of GCE electrode expressed altered current responses with respect to unmodified GCE as shown in Figure 23a. Stable current responses observed during 10 cycle recording indicate well reproducibility of the measurements using rGO/MoS_2 modified electrode.

CV voltammograms were further used to characterize the electron transfer kinetics. The influence of scan rate on current responses was demonstrated using rGO/MoS_2 modified electrode in the scan rate range of 10 to 150 mV s^{-1}. As can be observed in Figure 23b, peak currents reacted positively, increasing their values with increasing scan rate. According to highly linear dependence of peak current responses on square root of scan rate observed in Figure 23c, the charge transfer on the modified electrode surface was controlled by diffusion.

The rate of electron transfer on GCE electrode and electrode modified with rGO/MoS_2 was validated using the peak current values from CV voltammograms in Figure 23a. The clear evidence of faster electron mobility detected on rGO/MoS_2 modified electrode is depicted in its lower peak to peak separation when compared to bare GCE as shown Table 2.

Table 2. Table of ΔE values for rGO/MoS_2 modified GCE electrode and for bare GCE.

electrode	E_{pa} - E_{pc} (mV)
GCE	120
GCE + rGO/MoS_2	107

EIS measurement illustrated in Figure 23d further characterizes the difference in the charge transfer properties between the electrode modified with rGO/MoS_2 hybrid and bare GCE. Easy charge transfer free of any resistance is demonstrated by nearly no faradaic semicircle in case of modified electrode as compared with GCE electrode. Moreover, straight line observed on electrode modified with rGO/MoS_2 is reflection of low charge diffusion resistance and certain capacitive properties.

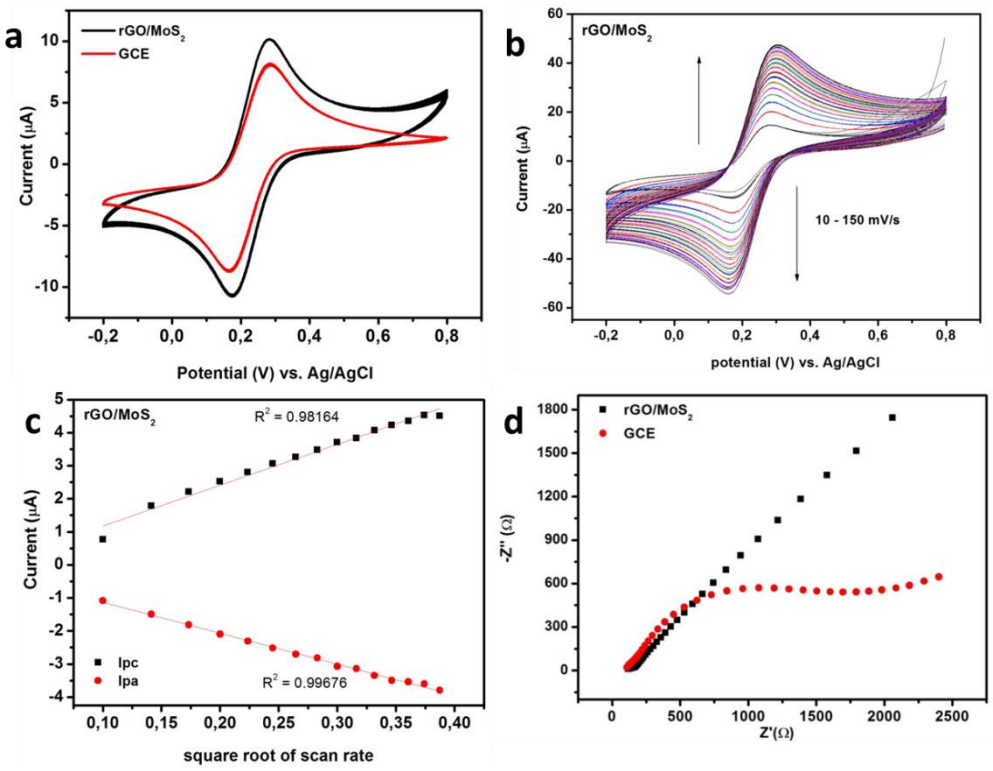

Figure 23. a) Cyclic voltammograms recorded by unmodified GCE and GCE modified with rGO/MoS_2, b) CV voltammograms recorded with GCE modified with rGO/MoS_2 at different scan rates (10 to 150 mV/s), c) Plot of anodic and cathodic currents vs. square root of scan rate measured by GCE modified with rGO/MoS_2, d) EIS measurements for rGO/MoS_2 modified electrode with respect to bare GCE.

All previously described results show that unique structure of N-doped graphene aerogels and rGO/MoS_2 composites can be consider as a new class of suitable and promising electrochemical materials. In summary, electrochemical properties of rGO-N and rGO/MoS_2 modified electrodes were determined with respect to unmodified glassy carbon electrodes and electrodes modified by rGO by both CV and EIS. All results indicating significant enhancement in current responses, lower charge resistance and optimal diffusion controlled redox behavior were obtained using modified electrode. It can be concluded that doping of rGO hydrogel with nitrogen led to improvement of electron transfer properties arising from better conductivity when compared to bare GCE. On the other hand, electrode modified with rGO indicated similar improvement as that modified with rGO-N. But it is worth mentioning that electrodes modified with rGO were not so stable and reproducible since the rGO tend to peel off from the electrode surface.

Similar results were obtained for electrode modified with rGO/MoS_2 hybrid. Higher current signals and low charge transport resistance with respect to GCE electrode were observed which can be ascribed to unique inner constitution of thy hybrid, where charge transfer is significantly enhanced. Moreover, among all three employed modifications the best reproducibility of the redox reaction occurring on the electrode/electrolyte interface was reached when rGO/MoS_2 hybrid was used for modification, which again confirms very well constituted electron paths network.

7.3. Application of rGO-N modified electrode for ascorbic acid and dopamine determination

Due to overall improvement of electrochemical behavior, rGO-N was chosen for further testing of its applicability in sensing. Ascorbic acid (AA) and dopamine (DA) were chosen as target molecules. Both are known as abundant substances occurring in human body and up certain levels can easily cause serious diseases such as Parkinson´s disease or cancer. They are targets of daily determinations as preventive controls and diagnosis purposes in hospitals. Their high overpotentials and hard separation of signals when using classical electrodes[12,56] create an ideal opportunity for application of modified electrodes with advanced detection abilities.

The sensing measurements were carried out at the same potentiostat, in the same electrode set-up, with the same drop-coating method and water dispersion concentrations as

described previously. Solutions of AA and DA were prepared in the phosphate buffer solution (PBS) of pH 7. Measurements were performed using cyclic voltammetry (CV) and difference pulse voltammetry (DPV).

First of all, CV was used in order to see the behavior of AA and DA using modified electrodes with respect to unmodified one as can be seen in Figure 24a,b. It was observed that at both modified electrodes, AA is detected at much lower overpotentials when compared to bare GCE (see Fig. 24a): 0V for rGO and rGO-N modified GCE while 0.63V for unmodified GCE. This effect could be probably ascribed to faster electron transfer provided by modified electrode that was already observed during the electrochemical characterization of materials. Importantly, sharp and well defined peak of AA is only observed when using GCE modified with rGO-N. In the case of DA, it was observed that the modified electrodes showed almost the same overpotential (around 0.42 V) with respect to bare GCE signal (0.52 V). On the other hand, rGO-N modified electrodes offered well defined peak with two times higher current response than that of bare GCE (Fig. 24b). Two distinguishable peaks observed in case of undoped rGO are most probably due to the DA decomposition during the measurement.

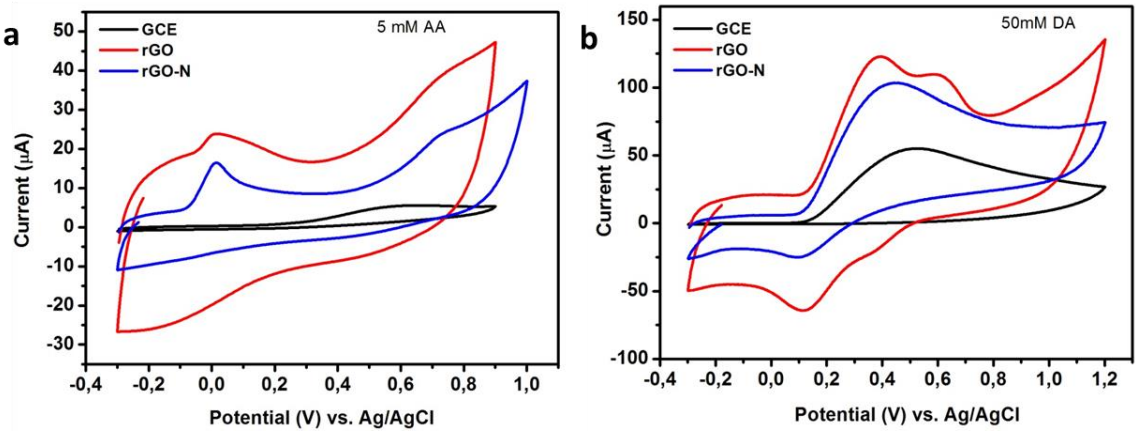

Figure 24. a) CV performance of the rGO-N modified electrode towards oxidation of 5 mM ascorbic acid with respect to rGO and GCE, b) CV performance of the rGO-N modified electrode towards oxidation of 50 mM dopamine with respect to rGO and GCE.

The calibration plots recorded by DPV showed good linear relationship between peak currents and the concentration of AA (Fig.25a) in the range of 10 – 50mM. For DA (Fig.25b) the relationship in the range of 0.1 – 1mM showed linear relationship up to 0.8mM and further decrement was probably caused by saturation of the electrode. Nonetheless, these

results together with above described improved catalytic properties towards AA and DA detection signals when compared to GCE can be considered as promising for applicability of rGO-N in analytical applications.

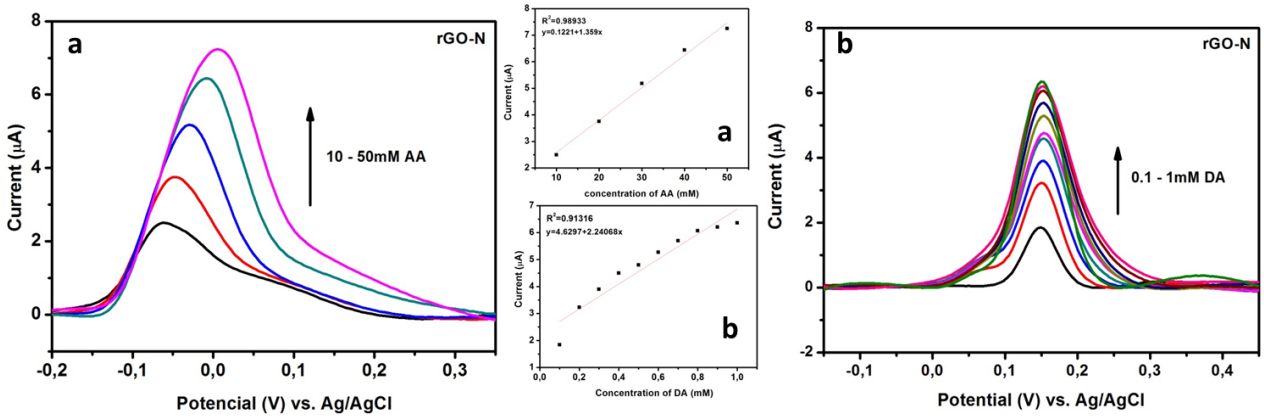

Figure 25. Calibrations of AA and DA performed on rGO-N modified electrode. a) Calibration plots of AA in the range of 10 – 50mM. Inset shows plots of peak currents as a function of AA concentration, b) Calibration plots of DA in the range of 0.1 – 1mM. Inset shows plots of peak currents as a function of DA concentration.

As next step, simultaneous determination of both AA and DA from their mixture was monitored either by CV or DPV using rGO-N modified electrode as shown in Figure 26a,b. In this experiment, very small concentrations of DA were added into 1 mM AA. Additions of DA into AA solution can be clearly determined as well separated peaks in higher overpotential. Further additions are well reflected in peak current increments in contrast to constant peak current of AA. Such simultaneous determination of two analytes from their mixture is very profitable and not very commonly obtained.

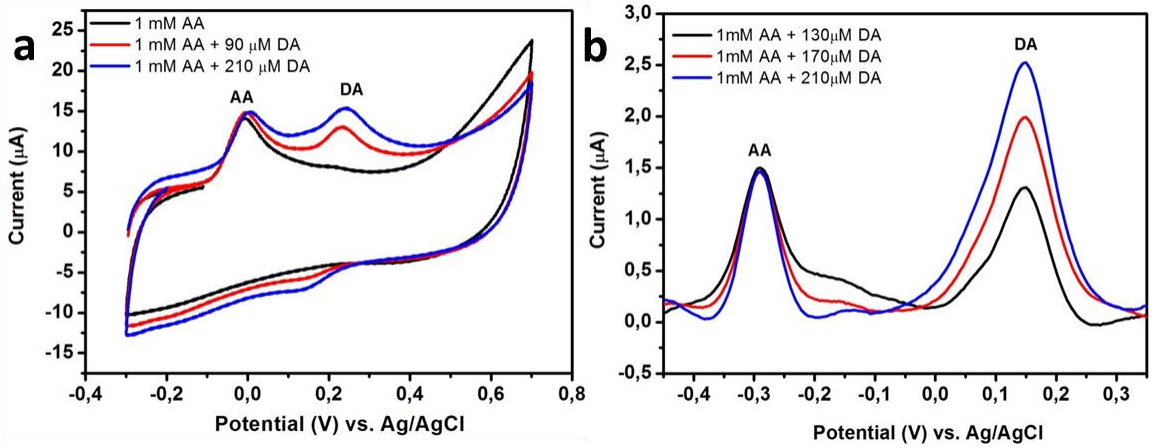

Figure 26. a) CV voltammograms of rGO-N modified electrode in 1mM AA and in mixture of 1mM AA with 90, 210 μM DA, b) DPV voltammograms of rGO-N modified electrode in mixture of 1mM AA with 90, 130, 170 μM DA.

Summary

The aim of the work was to synthesize two macroscopic graphene nanostructures: nitrogen doped reduced graphene oxide aerogel (rGO-N) and rGO/MoS_2 hybrid. These materials were prepared by solvothermal approach using GO as a main component. The detailed characterization of these materials helped to reveal its composition and structural features. The brief discussion related to rGO-N and rGO/MoS_2 is given below.

For fabricating rGO-N, we performed hydrothermal approach adapted from Chen *et al.* followed by freeze drying. rGO/MoS_2 hybrid was prepared by solvothermal method adapted from Zhao *et al.* Both nanostructures possess conductive three-dimensional architecture consisting of crumbled rGO sheets functionalized with nitrogen containing functional groups in case of rGO-N, while MoS_2 nanoparticles in case of rGO/MoS_2. Such hybrid nanostructures were proved to enhance the response after glassy carbon electrode modification in redox systems and exhibited significantly lower charge transfer resistance owing to porous and 3D structure and electrically active dopants. Furthermore, results of electro-sensing activities of rGO-N aerogel demonstrate electrocatalytic activities towards ascorbic acid and dopamine showing lower overpotentials and higher peak currents. Finally, abilities of rGO-N for simultaneous detection of aforementioned analytes in mixture were also confirmed.

In future, I would like to focus on synthesizing controlled doping of nitrogen in graphene nanostructures by hydrothermal approach. These materials will be tested for electro-sensing of toxic materials and as active electrocatalysts for oxygen reduction reactions. Furthermore, for rGO/MoS_2 hybrid I would like to focus more on detection H_2O_2, biomolecules and as electrocatalysts for hydrogen evolution reaction.

Závěr

Cílem bakalářské práce bylo syntetizovat dvě makroskopické grafenové nanostruktury: dusíkem dopovaný aerogel redukovaného grafen oxidu (rGO-N) a rGO/MoS2 hybrid. Tyto materiály byly připraveny solvotermálními metodami využívající GO jako hlavní komponentu. Detailní charakterizace těchto materiálů pomohla k objasnění jejich složení a strukturních rysů. Stručná diskuze týkající se rGO-N a rGO/MoS_2 je uvedena níže.

Přípravu rGO-N jsme provedli za použití hydrotermální metody podle Chen et. al, a následnou lyofilizací. rGO/MoS_2 hybrid byl připraven solvotermální metodou podle Zhao et. al. Obě nanostruktury disponovaly vodivou třídimensionální architekturou, kde zvlněné a pomačkané vrstvy GO byly v případě rGO-N funkcionalizovány dusíkovými funkčními skupinami a v případě rGO/MoS_2 nanočásticemi MoS_2. Takovéto hybridy, použité jako modifikace pro uhlíkovou skleněnou elektrodu, prokázaly posílenou odezvu redoxního sytému a výrazně nižší resistenci vůči přenosu náboje. Za těmito výsledky stojí porézní 3D struktura a dopování elektricky aktivními látkami. Výsledky elektro-sensingové aktivity rGO-N aerogelu dále demonstrovaly katalytické aktivity pro detekci kyseliny askorbové a dopaminu, jež byly detekovány v nižších potenciálech a vyšších proudových odezvách. Nakonec byly prokázány schopnosti rGO-N aerogelu pro simultánní detekci výše zmíněných analytů z jejich směsi.

V budoucnu bych se chtěla zaměřit na syntézu grafenových nanostruktur za použití hydrotermální metody s kontrolovaně dopovaným dusíkem. Tyto materiály by byly testovány pro elektro-sensing toxických materiálů a také jako elektro katalyzátor pro kyslík redukující reakci. Mimoto bych se v rámci rGO/MoS_2 chtěla zaměřit na detekci H_2O_2, biomolekul a také na elektro katalýzu pro vodík generující reakci.

List of references

1. Royal, T. H. E., Academy, S. & Sciences, O. F. compiled by the Class for Physics of the Royal Swedish Academy of Sciences Graphene. *R. Swedish Acad. Sci.* **50005,** 0–10 (2010).

2. Geim, A. K. & Novoselov, K. S. The rise of graphene. *Nat. Mater.* **6,** 183–191 (2007).

3. Zbořil, R. *et. al.*. Graphene fluoride: A stable stoichiometric graphene derivative and its chemical conversion to graphene. *Small* **6,** 2885–2891 (2010).

4. Sahin, H., Leenaerts, O., Singh, S. K. & Peeters, F. M. GraphAne: From Synthesis to Applications. (2015). at <http://arxiv.org/abs/1502.05804>(date accessed: 2016-04-03)

5. Dreyer, D. R., Park, S., Bielawski, C. W. & Ruoff, R. S. The chemistry of graphene oxide. *Chem. Soc. Rev.* **39,** 228–240 (2010).

6. Dimiev, A. M. & Tour, J. M. Mechanism of graphene oxide formation. *ACS Nano* **8,** 3060–3068 (2014).

7. G, W. G. Processable Aqueous Dispersions of Graphene Nanosheets. *Nat. Nanotechnol.* **3,** 101 (2008).

8. Feng, X., Chen, W. & Yan, L. Reduced graphene oxide hydrogel film with a continuous ion transport network for supercapacitors. *Nanoscale* **7,** 3712–3718 (2015).

9. Huang, X. *et. al.*. Functional nanoporous graphene foams with controlled pore sizes. *Adv. Mater.* **24,** 4419–4423 (2012).

10. Xu, Y. *et. al.*. Solvated graphene frameworks as high-performance anodes for lithium-ion batteries. *Angew. Chem. Int. Ed. Engl.* **54,** 5345–50 (2015).

11. Woinska, M., Milowska, K. & Majewski, J. A. Ab initio modeling of graphene layer functionalized with boron and nitrogen. *AIP Conf. Proc.* **1566,** 143–144 (2013).

12. Xing, L. & Ma, Z. A glassy carbon electrode modified with a nanocomposite consisting of MoS2 and reduced graphene oxide for electrochemical simultaneous determination of ascorbic acid, dopamine, and uric acid. *Microchim. Acta* **183,** 257–263 (2016).

13. Chen, P. *et. al.*. Hydrothermal synthesis of macroscopic nitrogen-doped graphene hydrogels for ultrafast supercapacitor. *Nano Energy* **2,** 249–256 (2013).

14. Zhao, Y. *et. al.*. Well-constructed single-layer molybdenum disulfide nanorose cross-linked by three dimensional-reduced graphene oxide network for superior water splitting and lithium storage property. *Sci. Rep.* **5,** 8722 (2015).

15. Allen, M. J., Tung, V. C. & Kaner, R. B. Honeycomb carbon: A review of graphene. *Chem. Rev.* **110,** 132–145 (2010).

16. Mattevi, C., Kim, H. & Chhowalla, M. A review of chemical vapour deposition of graphene on copper. *J. Mater. Chem.* **21,** 3324–3334 (2011).

17. Geim, A. K. Graphene : Status and Prospects. **1530,** 1530–1535 (2010).

18. Nobel prize in Physics. at <http://www.nobelprize.org/nobel_prizes/physics/laureates/2010/> (date accessed: 2016-04-03)

19. Georgakilas, V. *Functionalization of Graphene*. (Wiley-VCH Verlag GmbH & Co. KGaA, 2014). doi:10.1002/9783527672790

20. Geim, A. & Novoselov, K. Graphene — the perfect atomic lattice. *R. Swedish Acad. Sci.* **181,** 1283 (2011).

21. Castro Neto, A. H., Peres, N. M. R., Novoselov, K. S. & Geim, A. K. The electronic properties of graphene. *Rev. Mod. Phys.* **81,** 109–162 (2009).

22. Adee, P. E. UnIted States Patent [191. (1974)].

23. Fuchs, J.-N. Dirac fermions in graphene and analogues: magnetic field and topological properties. *arXiv Prepr. arXiv1306.0380* 77 (2013). at <http://arxiv.org/abs/1306.0380> (date accessed: 2016-04-12)

24. Miró, P., Audiffred, M. & Heine, T. An atlas of two-dimensional materials. *Chem. Soc. Rev.* **43,** 6537–54 (2014).

25. Van Noorden, R. Production: Beyond sticky tape. *Nature* **483,** S32–3 (2012).

26. Zan, R., Ramasse, Q. M., Jalil, R. & Bangert, U. Atomic structure of graphene and h-BN layers and their interactions with metals. *Adv. graphene Sci.* 63 (2013). doi:10.5772/56640

27. Nicolosi, V., Chhowalla, M., Kanatzidis, M. G., Strano, M. S. & Coleman, J. N. Liquid Exfoliation of Layered Materials. *Science (80-.).* **340,** 1226419 (2013).

28. Huh, S. H. & Korea, S. Thermal Reduction of Graphene Oxide. *Phys. Appl. Graphene - Exp.* 73–90 (2011). doi:10.5772/14156

29. Stankovich, S. *et. al.*. Synthesis of graphene-based nanosheets *via* chemical reduction of exfoliated graphite oxide. *Carbon N. Y.* **45,** 1558–1565 (2007).

30. Shin, H.-J. *et. al.*. Efficient Reduction of Graphite Oxide by Sodium Borohydride and Its Effect on Electrical Conductance. *Adv. Funct. Mater.* **19,** 1987–1992 (2009).

31. Georgakilas, V. *et. al.*. Functionalization of graphene: Covalent and non-covalent approaches, derivatives and applications. *Chem. Rev.* **112,** 6156–6214 (2012).

32. Lee, D. W. *et. al.*. The structure of graphite oxide: Investigation of its surface chemical groups. *J. Phys. Chem. B* **114,** 5723–5728 (2010).

33. He, H., Klinowski, J., Forster, M. & Lerf, A. A new structural model for graphite oxide. *Chem. Phys. Lett.* **287,** 53–56 (1998).

34. Society, R. On the Atomic Weight of Graphite Author (s): B . C . Brodie Source : Philosophical Transactions of the Royal Society of London , Vol . 149 (1859), pp . 249- Published by : Royal Society Stable URL : http://www.jstor.org/stable/108699 Accessed : 30-03-2016 19 : 45 UTC. **149,** 249–259 (2016).

35. Poh, H. L. *et. al.*. Graphenes prepared by Staudenmaier, Hofmann and Hummers methods with consequent thermal exfoliation exhibit very different electrochemical properties. *Nanoscale* **4,** 3515 (2012).

36. Kube, M. & Ku, J. Synthetic routes contaminate graphene materials with a whole spectrum of unanticipated metallic elements. 1–6 (2014). doi:10.1073/pnas.1413389111

37. Hu, H., Zhao, Z., Wan, W., Gogotsi, Y. & Qiu, J. Ultralight and Highly Compressible Graphene Aerogels. *Adv. Mater.* **25,** 2219–2223 (2013).

38. Zhao, Y. *et. al.*. A versatile, ultralight, nitrogen-doped graphene framework. *Angew. Chemie - Int. Ed.* **51,** 11371–11375 (2012).

39. Shen, Y., Fang, Q. & Chen, B. Environmental Applications of Three-Dimensional Graphene-Based Macrostructures : Adsorption , Transformation , and Detection.(2015).

40. Han, Z. *et. al.*. Strengthening of graphene aerogels with tunable density and high adsorption capacity towards Pb2+. *Sci. Rep.* **4,** 5025 (2014).

41. Ma, Y. & Chen, Y. Three-dimensional graphene networks: Synthesis, properties and applications. *Natl. Sci. Rev.* **2,** 40–53 (2015).

42. Jung, S. M., Mafra, D. L., Lin, C.-T., Jung, H. Y. & Kong, J. Controlled porous structures of graphene aerogels and their effect on supercapacitor performance. *Nanoscale* **7,** 4386–93 (2015).

43. Zhao, Z., Wang, X., Qiu, J., Lin, J. & Xu, D. Three-Dimensional Graphene-Based Hydrogel / Aerogel Materials. **36,** 137–151 (2014).

44. Szab, T. *et. al.*. Evolution of Surface Functional Groups in a Series of Progressively Oxidized Graphite Oxides Evolution of Surface Functional Groups in a Series of Progressively Oxidized Graphite Oxides. 2740–2749 (2006). doi:10.1021/cm060258

45. Jiang, X., Ma, Y., Li, J., Fan, Q. & Huang, W. Self-Assembly of Reduced Graphene Oxide into Three-Dimensional Architecture by Divalent Ion Linkage. *J. Phys. Chem. C* **114,** 22462–22465 (2010).

46. Graphene, D. C. A Strong Integrated Strength and Toughness Arti fi cial Nacre Based on. 9511–9517 (2014).

47. Wang, X. *et. al.*. Heteroatom-doped graphene materials: syntheses, properties and applications. *Chem. Soc. Rev.* **43,** 7067–7098 (2014).

48. Geim, a K. & Grigorieva, I. V. Van der Waals heterostructures. *Nature* **499,** 419–25 (2013).

49. Dong, H. *et. al.*. Three-dimensional Nitrogen-Doped Graphene Supported Molybdenum Disulfide Nanoparticles as an Advanced Catalyst for Hydrogen Evolution Reaction. *Sci. Rep.* **5,** 17542 (2015).

50. Vasilescu, I. *et. al.*. Biosensors and Bioelectronics Molybdenum disulphide and graphene quantum dots as electrode modi fi ers for laccase biosensor. *Biosens. Bioelectron.* **75,** 232–237 (2016).

51. Amino-Functionalization of Graphene Sheets and the Fabrication of Their Nanocomposites_<http://wenku.baidu.com/view/c8162f639b6648d7c1c746c8.html###> (date accessed: 2016-04-03)

52. Panchakarla, L. S. *et. al.*. Synthesis, Structure and Properties of Boron and Nitrogen Doped Graphene. 12 (2009). doi:10.1002/adma.200901285

53. Qu, L., Liu, Y., Baek, J. B. & Dai, L. Nitrogen-doped graphene as efficient metal-free electrocatalyst for oxygen reduction in fuel cells. *ACS Nano* **4,** 1321–1326 (2010).

54. Li, S. M. *et. al.*. Controllable synthesis of nitrogen-doped graphene and its effect on the simultaneous electrochemical determination of ascorbic acid, dopamine, and uric acid. *Carbon N. Y.* **59,** 418–429 (2013).

55. Xie, B. *et. al.*. Hydrothermal synthesis of layered molybdenum sulfide/N-doped graphene hybrid with enhanced supercapacitor performance. *Carbon N. Y.* **99,** 35–42 (2016).

56. Sheng, Z.-H. *et. al.*. Electrochemical sensor based on nitrogen doped graphene: Simultaneous determination of ascorbic acid, dopamine and uric acid. *Biosens. Bioelectron.* **34,** 125–131 (2012).

57. Li, X., Wang, W., Zhang, L., Jiang, D. & Zheng, Y. Water-exfoliated MoS2 catalyst with enhanced photoelectrochemical activities. *Catal. Commun.* **70,** 53–57 (2015).

58. Huang, K. J., Wang, L., Li, J. & Liu, Y. M. Electrochemical sensing based on layered MoS2-graphene composites. *Sensors Actuators, B Chem.* **178,** 671–677 (2013).

59. Zan, W., Geng, W., Liu, H. & Yao, X. Influence of interface structures on the properties of Molybdenum Disulfide/Graphene composites: a density functional theory study. *J. Alloys Compd.* **649,** 961–967 (2015).

60. Song, I., Park, C. & Choi, H. C. Synthesis and properties of molybdenum disulphide: from bulk to atomic layers. *RSC Adv.* **5,** 7495–7514 (2015).

61. Splendiani, A. *et. al.*. Emerging photoluminescence in monolayer MoS2. *Nano Lett.* **10,** 1271–1275 (2010).

62. Yoffe, A. D. Low-dimensional systems: Quantum size effects and electronic properties of semiconductor microcrystallites (zero-dimensional systems) and some quasi-two-dimensional systems. *Adv. Phys.* **51,** 799–890 (2002).

63. Cao, T. *et. al.*. Valley-selective circular dichroism of monolayer molybdenum disulphide. *Nat. Commun.* **3,** 887 (2012).

64. Cyklická voltametrie. doi:10.1017/CBO9781107415324.004

65. Peng, J. & Weng, J. One-pot solution-phase preparation of a MoS2/graphene oxide hybrid. *Carbon N. Y.* **94,** 568–576 (2015).

66. Li, Y. *et. al.*. MoS2 nanoparticles grown on graphene: An advanced catalyst for the hydrogen evolution reaction. *J. Am. Chem. Soc.* **133,** 7296–7299 (2011).

67. Marcano, D. C. *et. al.*. Improved Synthesis of Graphene Oxide. *ACS Nano* **4,** 4806–4814 (2010).

68. Kim, N. H., Kuila, T. & Lee, J. H. Simultaneous reduction, functionalization and stitching of graphene oxide with ethylenediamine for composites application. *J. Mater. Chem. A* **1,** 1349 (2013).

69. Samadaei, F., Salami-Kalajahi, M., Roghani-Mamaqani, H. & Banaei, M. A structural study on ethylenediamine- and poly(amidoamine)-functionalized graphene oxide: simultaneous reduction, functionalization, and formation of 3D structure. *RSC Adv.* **5,** 71835–71843 (2015).

70. Yang, H. *et. al.*. Influences of graphene oxide support on the electrochemical performances of graphene oxide-MnO2 nanocomposites. *Nanoscale Res. Lett.* **6,** 531 (2011).

71. Dresselhaus, M. S., Jorio, A. & Saito, R. Characterizing Graphene, Graphite, and Carbon Nanotubes by Raman Spectroscopy. *Annu. Rev. Condens. Matter Phys* **1,** 89–108 (2010).

72. Xue, B., Zhu, J., Liu, N. & Li, Y. Facile functionalization of graphene oxide with ethylenediamine as a solid base catalyst for Knoevenagel condensation reaction. *Catal. Commun.* **64,** 105–109 (2015).

73. Qin, P. *et. al.*. In situ growth of double-layer MoO3/MoS2 film from MoS2 for hole-transport layers in organic solar cell. *J. Mater. Chem. A* **2,** 2742 (2014).

74. Kim, S.-K., Wie, J. J., Mahmood, Q. & Park, H. S. Anomalous nanoinclusion effects of 2D MoS2 and WS2 nanosheets on the mechanical stiffness of polymer nanocomposites. *Nanoscale* 7430–7435 (2014). doi:10.1039/c4nr01208a

75. Otyepková, E., Otyepka, M. Fundamentals of physicochemical methods - study materials. <http://fch.upol.cz/skripta/zfcm_pred/> (date accessed: 2015-01-05)

76. Heath, J. Energy Dispersive Spectroscopy 2nd Ed. 32 (2015).

77. Center for materials crystallography, Aarhus University. at <http://cmc.chem.au.dk/facilities/elemental-analysis/> (date accessed: 2016-05-03)